



Semnan University

Mechanics of Advanced Composite Structures

journal homepage: <http://MACS.journals.semnan.ac.ir>

Response of Agglomerated SWCNT Reinforced Nanocomposite Plate under Hygro-Thermal Loading

M. C. Maurya ^{a*}, S. M. Ali Jawaid ^a, A. Chakrabarti ^b^a Department of Civil Engineering, Madan Mohan Malaviya University of Technology, Gorakhpur-273010, India^b Department of Civil Engineering, Indian Institute of Technology, Roorkee-247667, India

KEYWORDS

CNT;
Agglomeration;
High-order shear deformation theory;
Hygrothermal environment.

ABSTRACT

In this study, the hygrothermal flexural behavior of a nanocomposite plate reinforced with carbon nanotubes is analyzed. The Eshelby-Mori-Tanaka (EMT) technique, a micromechanical model based on two parameters, is used to calculate the nanocomposite plate's real mechanical properties. The model incorporates the effects of clustering. The virtual work notion from higher-order shear deformation theory (HSDT) is used to develop the governing differential equations. After that, a C^0 continuous isoparametric Lagrangian FE model with seven nodal unknowns is used to apply the present method with the FEM. Creating the finite element code allows one to calculate the nanocomposite plate's deflection. To make sure that the method works, the results are compared to numerical results that have already been published. The flexural response of the nanocomposite plate with agglomerated carbon nanotubes (CNTs) is next analyzed by performing extensive parametric studies to determine the impacts of agglomeration degree, moisture, temperature, the volume percentage of CNTs, and various aspect ratio.

1. Introduction

The study of Iijima [1,2] enabled scientists to appreciate the vast potential of Carbon Nanotubes (CNTs) and attracted the curiosity of a large number of researchers who set out to find a practical use for CNTs that would benefit from them. Since their discovery, carbon nanotubes have been considered the ideal nanocomposite material for aerospace and mechanical engineering applications due to their excellent mechanical and thermal properties [3]. Functionally graded nanocomposite plates have gained popularity due to their better mechanical properties. Functionally graded nanocomposites can be used in several smart architectures [8]. Despite the many publications on the topic, CNT mechanical characteristics and characterization remain unsolved [4]. The literature provides several approaches to understand how these composites perform mechanically, and they are often employed for structural applications to improve dynamic response or buckling difficulties. Due to these considerations, CNT

insertion into the polymeric matrix with varied distributions and the agglomeration effect was investigated. An extended Rule of Mixture [5] can be used to determine the mechanical properties of a CNT-reinforced layer with orthotropic properties. Alibeigloo [6,7] utilized elasticity to study the dynamic and thermal behavior of CNT-based nanocomposite structures. These studies illustrate this methodology. Alibeigloo and Liew [6] and Alibeigloo [7] demonstrate these uses. Carbon nanotubes (CNTs) are a notable nanomaterial used in mechanical applications [9–15]. Due to their excellent mechanical, thermal, electrical, and physical properties, CNTs have many applications. Nanotechnology in medical, electronics, optics, and advanced composite materials [16–22] are examples.

Previous research [23–26] has shown that including even minute numbers of carbon nanotubes (CNTs) into the matrix of a polymer composite is capable of producing sizeable gains in the composite's bulk mechanical characteristics. CNTs, on the other hand, have a low bending stiffness due to the large aspect

* Corresponding author. Tel.: +91-9451800047
E-mail address: mcmce@mmmut.ac.in

ratios that they possess, which makes it simple for them to form clusters within the polymer matrix. So, carbon nanotube-reinforced composite (CNTRC) structures often have nanotubes that aren't spread out evenly or are clumped together. This makes it harder to improve the composite's modulus and strength. When figuring out the real properties of nanocomposite, it is important to take into account how agglomerates work. Shi et al. [27] came up with a theory for a micromechanics approach that took into account the effects of CNTs being bent and clumped together. It was shown that CNT agglomerates make CNT-reinforced composites much less stiff. Using a modified version of the Mori-Tanaka method. The authors Yu et al. [28] investigated how the useful properties of nanocomposites were affected by the morphology of the VGCF, the interphase between the nanofibers and the matrix, and the waviness of the nanofibers. Pourasghar et al. [29] investigated the impact of CNT agglomeration on the vibrational behavior of cylindrical, four-parameter continuously graded nanocomposite panels with randomly oriented CNTs using 3D elasticity theory. Nejati et al. [30] studied the flexural and vibrational behavior of functionally graded nanocomposite shells by employing the approach of generalized differential quadrature. Using GDQ as a low-cost method to analyze rotating conical shells composed of composite materials was believed to provide a very realistic depiction of their operation. GDQ technique was used by the effect of CNT agglomeration on nanocomposite conical shells was investigated by Kamarian et al. [31]. Calculating the properties of the nanocomposite shell based on the concept of "equivalent fibers" was accomplished through the use of the two-parameter Eshelby-Mori-Tanaka method. They found that the wave numbers of the fundamental frequencies were unaffected by the two agglomeration parameters, but that the natural frequencies were quite sensitive to the agglomeration parameters. It was also pointed out that as the number of cities grew, the natural frequencies went down. Recent research conducted by Daghigh and Daghigh [32] utilized analytical Navier's approach to investigate the size-dependent free vibration response of carbon nanotube reinforced nanocomposite plate that had nanotube clumping and polymethyl methacrylate (PMMA) as the matrix. When CNT agglomerates were present, it was found that the nanoplate's natural frequencies dropped by a lot. The Mori-Tanaka approach was utilized by Nasihatgozar et al. [33] studied the influence of CNT volume fraction, geometrical ratios, and loading conditions on the buckling behavior of piezoelectric cylindrical carbon nanotube-

reinforced composite panels. The biaxial buckling [34] behavior of simply supported functionally graded sandwich plates with randomly dispersed agglomerated carbon nanotubes was investigated with the help of Navier's solution. In order to make an estimation of the qualities of the material, the Mori Tanaka method was utilized. Lei et al. [35] studied the impact of carbon nanotube distribution, boundary conditions, and geometrical factors on the nonlinear flexural response of FG-CNT plate using the FSDT theory in conjunction with the method proposed by kp-Ritz based on element free approach. They discovered that the different forms of CNT dispersion have a significant impact on the nonlinear response shown by CNT-based composite plates. Zhang et al. [36] investigated the nonlinear flexural response of FG nanocomposite thick plates that were supported by a Pasternak foundation by using the improved moving least-squares Ritz method in conjunction with the modified Newton-Raphson technique. This research was done in a later study. It was discovered that the specifications of the elastic basis as well as the skew angle had a significant impact on the amount of nonlinear bending that the functionally graded nanocomposite plates displayed. Heydari et al. [37] studied the nonlinear bending response of FG-based nanocomposite plates resting on an orthotropic medium. This was done in a similar fashion. The impacts of varying patterns of single-walled carbon nanotube (SWCNT) distribution, CNT volume fractions, and elastomeric media were investigated by the researchers. Mehar et al. [38] have looked at the vibration properties of carbon-nanotube-reinforced polymer-based composites in a lot of detail, both theoretically and through experiments. Moghadam et al. [39] investigated the CNT agglomeration effect on the residual stresses in a fiber-reinforced nanocomposite. In order to estimate the residual stress that was caused by the thermal environment, an analytical solution was utilized, which was founded on the traditional laminate theory.

The results of these studies established nonlocal theories that are applicable to a diverse set of structures. In the research literature, carbon nanotubes reinforced composite (CNTRC) nanoplates have been the subject of a comparatively small number of experiments. Researchers Ravari et al. [40] used Mindlin's strain gradient theory to conduct their research on functionally graded carbon nanotube-based composite plates. When nonlocal influences were taken into account, the anticipated effective moduli of nanoplates were found to be higher than those obtained through the use of classical (local) elasticity. Phung-Van et al. [41] employed an isogeometric analysis to study the effect of

various CNT distributions along with alterations to nonlocal parameter values on the static and dynamic behavior of a functionally graded nanocomposite plate. This study was conducted in a similar manner as the previous one. They found that a rise in a nonlocal parameter caused a reduction in natural frequencies, and they reported this finding. Thanh et al. [42] did an isogeometric study of functionally graded nanocomposite plates using the rule of mixtures. This analysis was done in order to determine how the length scale influences the nanoplates. They did this by using the same numerical technique while employing a modified version of the coupled stress theory. Mohammadimehr et al. [59] investigated bending, buckling, and free vibration behaviors of microcomposite plates reinforced by functionally graded single-walled carbon nanotube (FG-SWCNT) under hydro-thermal environments by using third-order shear deformation theory (TSDT) and modified strain gradient theory (MSGT). Barai et al. [60] in their study developed a two-scale micromechanical model to analyze the effect of CNT agglomeration and interface condition on the plastic strength of CNT/metal composites. Shen et al. [61] used an energy approach in the framework of molecular mechanics to evaluate the local and global deformations of an SWCNT in a unified manner. The study was carried out under four loading conditions: axial tension, torsional moment, in-plane biaxial tension, and in-plane pure shear, respectively, from which the closed-form expressions for the longitudinal Young's modulus, major Poisson's ratio, longitudinal shear, plane strain bulk, and in-plane shear moduli were obtained. Dai et al. [64] examined the hygrothermo-mechanical behaviors of a porous nanocomposite annular plate with varied thicknesses while taking CNT aggregation into consideration. Brischetto [65] utilizes Carrera's Unified Formulation (CUF) to conduct an investigation on the effects that hygrothermal stress has on the bending of multilayered composite plates. Mahapatra et al. [66, 67] examined the combined effect of thermal moisture on the static behavior of cylindrical panels and ultimately concluded that these conditions have a substantial impact. They used a micromechanical model based on nonlinear finite elements to achieve this result. The impacts of thickness ratio, lamination scheme, and support conditions are explored in depth under a variety of various sets of hygrothermal circumstances. Daghig et al. [68] investigated the nonlocal bending and buckling behavior of agglomerated CNT-based nanocomposite plates resting on a Pasternak foundation. The flexural and buckling response of the nanocomposite plate with aggregation of CNTs was studied extensively, and

the implications of the parameters were discussed. Dahiya et al. [69] presents an article on critical reviews of the different synthesis techniques of graphene-reinforced nanocomposites (Gr-NCs).

The overall purpose of this review is to critically review the existing development in Gr-NCs and provide a comprehensive overview of Gr-NCs. The review results show that by reinforcing graphene and its derivatives into the matrix, the resulting composite may enhance functionality and explore new NCs for various nanostructures. Shaikh et al. [70] studied new and advanced basalt-carbon epoxy hybrid laminated composites under static loading using finite element analysis and various properties of basalt-carbon epoxy hybrid laminated composites such as tensile and compression strength, flexure strength, interlaminar, and in-plane shear strength were evaluated through different static test simulations. Finally, the specimens having different stack-up sequences and fibre orientations were analyzed for failure based on Tsai-Wu failure criteria using commercial finite element software. Dwaikat et al. [71] observed that the stochastic nature and the variability of the constituents of nanocomposites materials affect the predictability of their properties. Georgantzinos et al. [72] used a multi-scale framework for the estimation of the hygro-thermo-mechanical elastic performance of laminated composite structures with single-walled carbon nanotube (SWCNT) inclusions. In this study Halpin-Tsai equations were utilized for the estimation of the homogenized stiffness characteristics of the nano-reinforced matrix, considering constant levels of SWCNT agglomeration, orientation, and waviness and taking into account nanoscopic size-dependent characteristics of SWCNTs. Finally, the mechanical properties of laminated composites reinforced by CNTs were predicted using a multiscale-based finite element method considering various hygro-thermo-mechanical factors. Chen et al. [73] studied the mechanical behavior of double-walled carbon nanotubes (DWCNTs) under temperature gradients and electrical fields based on the nonlocal reddy beam model, focusing on the free vibration of DWCNTs. Alavi et al. [74] presents the first application of the Meshless local Petrov-Galerkin (MLPG) method for 3-D elasticity analysis of moderately thick rectangular laminated plates.

The majority of the earlier research made the assumption that the CNTs' orientations were linear and aligned, and they determined the mechanical properties of the CNTs by applying the rule of mixing. This was done for the sake of simplicity. However, these methods do not take into consideration wavy CNTs or agglomeration

of CNTs, which is quite prevalent even at low CNT volume fractions. Agglomeration of CNTs can be quite severe.

In light of the extensive literature study that was presented before, it can be said that the current article is organized in a way that makes it easier to incorporate the CNTs agglomeration effect. It is clear that CNTs have a propensity to aggregate in order to achieve low-volume fraction distribution. If the effect that was just described is not taken into account, then the conclusions that are drawn about the structures that are constructed using these CNT materials will be incorrect. Flexural investigation of a CNTRC nanocomposite plate that contains agglomerated CNTs is presented in the current study.

For the purpose of capturing the effective material properties of a CNT-based nanocomposite plate containing well-dispersed CNTs and CNT agglomeration, the Eshelby-Mori-Tanaka method is utilized. The governing equations are established and solved by applying the FE method while employing Reddy's HSDT model. This is done by putting into practice the virtual work principle. Considerations of the effects of aggregation parameters, CNT volume %, temperature, moisture, and plate aspect ratio on the overall flexural response of nanocomposite plates are presented.

2. Material Modeling

Material modeling plays an important role in any structural analysis. The application of CNT-reinforced composite structures demands to development of detailed modeling of the effective material properties of such composite at the macroscopic level. Because molecular dynamics or other atomistic models are computationally intensive, micromechanical methods are used to describe the behavior of these materials in this work. Material modeling of FG-CNTRC is presented using the Mori-Tanaka method considering the effect of agglomeration of CNT for various types of CNT distributions.

2.1. Material Modeling of Functionally Graded CNT Reinforced Composite

FG-CNTRC is assumed to consist of an isotropic matrix (epoxy resin) and fiber (carbon nanotubes), with material quality grades along the thickness direction of the plate according to the linear distribution of CNT volume fraction as shown in Fig. 1.

CNT volume fractions (V_{cnt}) in three types of functionally graded nanocomposite plates are given as follows:

$$V_{CNT} = V_{cnt}^* \quad (UD) \quad (1)$$

$$V_{cnt} = 2 \left(1 - \frac{2|z|}{h} \right) V_{cnt}^* \quad (FG-O)$$

$$V_{cnt} = 2 \left(\frac{2|z|}{h} \right) V_{cnt}^* \quad (FG-X)$$

$$V_{cnt}^* = \frac{w_{cnt}}{w_{cnt} + \frac{\rho_{cnt}}{\rho_m} - \left(\frac{\rho_{cnt}}{\rho_m} \right) w_{cnt}} \quad (2)$$

where,

w_{cnt} = mass fraction of carbon nanotubes and

ρ_{cnt} = mass density of carbon nanotube

ρ_m = mass density of the matrix

The material properties can be determined for the linear material property fluctuation by putting the value of V_{cnt}^* into Eq. (1) for linear material property variation.

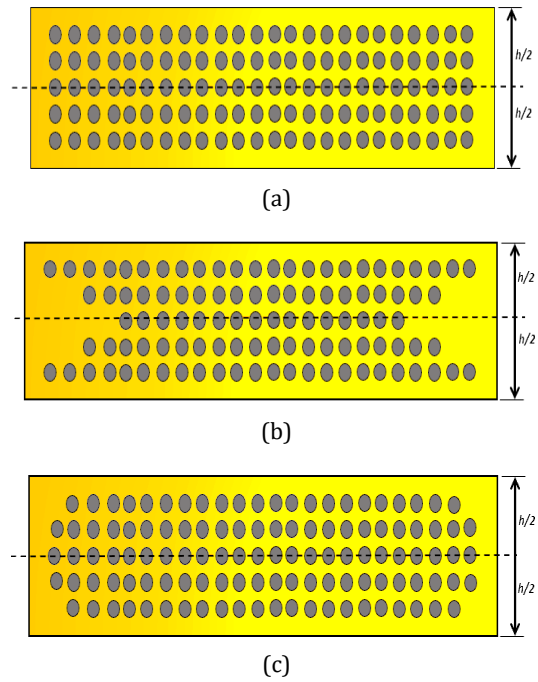


Fig. 1. (a) Uniformly distributed CNT nanocomposite plate, (b) X-Shape distributed CNT nanocomposite plate, (c) O-Shape distributed CNT nanocomposite plate [74].

2.2. Modeling of Nanocomposite Material

A variety of different micromechanical models have been presented in order to provide an estimation of the material properties of the nanocomposite. Estimating the elastic characteristics of the corresponding fiber/polymer material is accomplished by the application of the Mori-Tanaka method in this line of investigation.

The equivalent inclusion average stress approach, also known as the Eshelby-Mori-Tanaka method, is founded on two concepts: the idea of equivalent elastic inclusion developed by Eshelby and the concept of average stress inside the matrix developed by Mori-Tanaka. Together, these two ideas form the basis for the technique. The tensor of effective elastic moduli C of CNTRCs has been revised as follows according to Benveniste's [45] work:

$$C = C_m + V_{cnt} \langle (C_r - C_m) A \rangle \left(\frac{V_m I + V_{cnt} \langle A_r \rangle}{V_{cnt} \langle A_r \rangle} \right)^{-1} \quad (3)$$

where,

- I = fourth-order unit tensor
- C_m = matrix stiffness tensors
- C_r = equivalent fiber stiffness tensors

The angle brackets in their overall configuration represent an average of all conceivable orientations for the inclusions A_r is the tensor of the concentration of dilute mechanical strain, and it can be calculated as follows:

$$A_r = [I + S(C_m)^{-1}(C_r - C_m)]^{-1} \quad (4)$$

where S is the Eshelby tensor of the fourth order as given by Eshelby and Mura [8,10].

Here, a single-walled carbon nanotube having a solid cylinder of 1.424 nm diameter with (10,10) chirality index [46] is used for the analysis.

2.2.1. Randomly Oriented Straight CNTs Reinforced Composite

Straight carbon nanotube orientation is defined by two Euler angles α and β , denoted by the arrows in Fig. 2. As a result, the base vectors \vec{e}_i of the global $(0-x_1, x_2, x_3)$ coordinate system and the base vectors of \vec{e}'_i the local coordinate system, $(0-x'_1, x'_2, x'_3)$ are produced, which are related through the transformation matrix g , as follows:

$$\vec{e}_i = g \vec{e}'_i \quad (5)$$

where g is given by:

$$g = \begin{bmatrix} \cos \beta & -\cos \alpha \sin \beta & \sin \alpha \sin \beta \\ \sin \beta & \cos \beta \cos \alpha & -\sin \alpha \cos \alpha \\ 0 & \sin \alpha & \cos \alpha \end{bmatrix} \quad (6)$$

It is possible to characterize the orientation distribution of carbon nanotubes in composites by a probability density function $p(\alpha, \beta)$ that meets the normalizing condition.

The CNT orientation distribution in composites can be characterized by a probability density function $p(\alpha, \beta)$ that satisfies the normalization condition.

$$\int_0^{2\pi} \int_0^{\pi/2} p(\alpha, \beta) \sin \alpha d\alpha d\beta = 1 \quad (7)$$

Considering the random CNT orientation, the density function for this case is,

$$p(\alpha, \beta) = \frac{1}{2\pi} \quad (8)$$

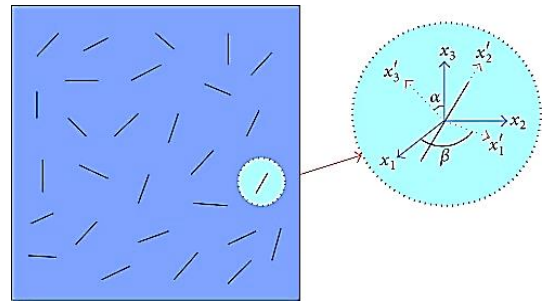


Fig. 2. Randomly oriented, straight CNTs make up a representative volume element (RVE) [43].

The Hill's elastic moduli for the reinforcing phase were computed by determining the equivalence of the two matrices that are presented further down [47]:

$$C_r = \begin{bmatrix} n_r & l_r & l_r & 0 & 0 & 0 \\ l_r & k_r + m_r & k_r - m_r & 0 & 0 & 0 \\ l_r & k_r - m_r & k_r + m_r & 0 & 0 & 0 \\ 0 & 0 & 0 & p_r & 0 & 0 \\ 0 & 0 & 0 & 0 & m_r & 0 \\ 0 & 0 & 0 & 0 & 0 & p_r \end{bmatrix} \quad (9)$$

$$= \begin{bmatrix} \frac{1}{E_L} & \frac{-v_{TL}}{E_T} & \frac{-v_{2L}}{E_Z} & 0 & 0 & 0 \\ \frac{-v_{LT}}{E_L} & \frac{1}{E_T} & \frac{-v_{2T}}{E_Z} & 0 & 0 & 0 \\ \frac{-v_{LZ}}{E_L} & \frac{-v_{TZ}}{E_T} & \frac{1}{E_Z} & 0 & 0 & 0 \\ 0 & 0 & 0 & \frac{1}{G_{TZ}} & 0 & 0 \\ 0 & 0 & 0 & 0 & \frac{1}{G_{TZ}} & 0 \\ 0 & 0 & 0 & 0 & 0 & \frac{1}{G_{LT}} \end{bmatrix}^{-1}$$

where k_r , l_r , m_r , n_r , and p_r represent the Hill's elastic moduli of the composite's reinforcing phase (CNTs) found by taking the inverse of the compliance matrix of the similar fibre.

In order to determine the properties of the composite, such as E_L , E_T , E_Z , G_{LT} , G_{TZ} , G_{TZ} , and v_{LT} , which may be established using the rule of mixture method, the first step is to determine the

properties of the composite by performing MD simulation or multiscale FEM analysis [48] on the nanocomposite. This can be done by simulating the composite on multiple scales.

The composite is isotropic when the CNTs are orientated in the matrix randomly and the bulk modulus K and shear modulus G are derived as follows:

$$K = K_m + \frac{V_{cnt}(\delta_r - 3K_m\alpha_r)}{3(V_m + V_{cnt}\alpha_r)} \quad (10)$$

$$G = G_m + \frac{V_{cnt}(\eta_r - 2G_m\beta_r)}{2(V_m + V_{cnt}\beta_r)} \quad (11)$$

The matrix's bulk and shear moduli are denoted by K_m and G_m , respectively.

$$\alpha_r = \frac{3(K_m + G_m) + k_r - I_r}{3(G_m + k_r)} \quad (12)$$

$$\beta_r = \frac{1}{5} \left[\frac{4G_m + 2k_r + I_r}{3(G_m + k_r)} + \frac{4G_m}{G_m + p_r} + \frac{2[G_m(3K_m + G_m) + G_m(3K_m + 7G_m)]}{G_m(3K_m + G_m) + m_r(3K_m + 7G_m)} \right] \quad (13)$$

$$\delta_r = \frac{1}{3} \left[n_r + 2I_r + \frac{(2k_r + n_r)(3k_m + 2G_m - I_r)}{G_m + k_r} \right] \quad (14)$$

$$\eta_r = \frac{1}{5} \left[\frac{\frac{2}{3}(n_r - I_r) + \frac{8G_m p_r}{G_m + p_r} + \frac{8m_r G_m (3K_m + 4G_m)}{3K_m(m_r + G_m) + G_m(7m_r + G_m)}}{2(k_r - I_r)(2G_m + I_r)} + \frac{1}{3(G_m + k_r)} \right] \quad (15)$$

In conclusion, the mechanical properties of the nanocomposites, which include E , ν , ρ , α , and β may be broken down into the following categories:

$$E = \frac{9KG}{3K + G} \quad (16)$$

$$\nu = \frac{3K - 2G}{6K + 2G} \quad (17)$$

In addition, V_{cnt} and V_m stand for the CNT volume fraction and matrix, respectively, and ensure that the equation $V_{cnt} + V_m = 1$ is satisfied. In a similar way, the mass density ρ is determined as follows:

$$\rho = \rho_{cnt}V_{cnt} + \rho_mV_m \quad (18)$$

$$\alpha = \left(\frac{E + 4\nu K(1 + \nu)}{E + 4\nu K(1 + \nu)^2} \right) \quad (19)$$

$$\left(\frac{V_{cnt}E_{11}^{CNT}\alpha_{11}^{CNT} + (1 - V_{cnt})E_m\alpha_m}{V_{cnt}E_{11}^{CNT} + (1 - V_{cnt})E_m} \right)$$

$$\beta = \left(\frac{E + 4\nu K(1 + \nu)}{E + 4\nu K(1 + \nu)^2} \right) \quad (20)$$

$$\left(\frac{V_{cnt}E_{11}^{CNT}\beta_{11}^{CNT} + (1 - V_{cnt})E_m\beta_m}{V_{cnt}E_{11}^{CNT} + (1 - V_{cnt})E_m} \right)$$

here, β and α are the coefficients of thermal and moisture expansion, and ΔT and ΔH are the thermal and moisture variations, which are given by $T = T_{(z)} - T_0$ and $H = H_{(z)} - H_0$. Also, T_0 and H_0 stand for the ambient temperature and humidity, which are both kept at 0 K and 0 wt% H₂O in this case. Also, $T_{(z)}$ and $H_{(z)}$ show a linear change in temperature and moisture along the direction of the plate's thickness [49]:

$$T_{(z)} = T_b + \Delta T_{tb}(0.5 + z/h) \quad (21)$$

$$H_{(z)} = H_b + \Delta H_{tb}(0.5 + z/h) \quad (22)$$

In the above equations, the subscripts t and b represent the top and bottom of the model, respectively. Next, the T_{tb} and H_{tb} represent the difference in temperature and humidity between the top and bottom. Specifically, $\Delta T_{tb} = T_t - T_b$ and $\Delta H_{tb} = H_t - H_b$ stand for ΔT_{tb} and ΔH_{tb} , respectively.

2.2.2. Agglomeration of CNTs

A large proportion of carbon nanotubes in carbon nanotube-reinforced composites has been found to be concentrated in agglomerates. Nanotubes agglomerate into bundles as a result of the van der Waals attractive interactions between them. After determining the material properties without taking into consideration the impact that agglomeration has, a new micromechanics model is developed and applied to a randomly oriented, agglomerated nanotube-reinforced polymer composite in order to calculate the effective material properties of an SWCNT-reinforced polymer composite while including the impact of CNT agglomeration. This work investigates the effect of CNT aggregation on the elastic characteristics of the randomly oriented nanocomposite, and it does so by using a two-parameter agglomeration model. As can be seen in Fig. 3, areas of concentrated nanotubes are regarded as inclusions because they possess elastic properties that are distinct from those of the material that surrounds them.

2.2.2.1. Two Parameter Agglomeration Model

In polymer matrix, the major cause of agglomeration of carbon nanotubes is the small diameter, due to which the elastic modulus gets reduced and the aspect ratio increases in the radial direction and hence produces low bending strength. In order to produce CNT-reinforced composites with the characteristics that are desired, it is essential that the carbon nanotubes be distributed evenly throughout the matrix. Here, a micromechanical model has been built to examine the effect of agglomerated CNTs on the effectiveness of carbon nanotube-enhanced elastic modules.

Shi et al. [27] found that a substantial number of CNTs are concentrated in aggregates in the 7.5 % concentration sample. Carbon nanotubes are found to be unevenly distributed in the substrate, with a few areas having CNT concentrations larger than the average volume fraction. As illustrated in Fig. 3, these areas containing concentrated carbon nanotubes are considered spherical in this section and are referred to as 'inclusions' having a mix of varying elasticity characteristics from the surrounding material.

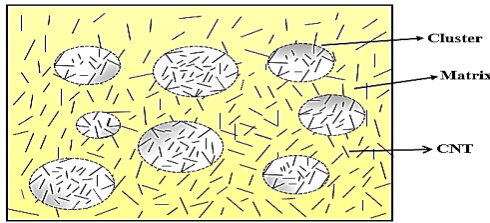


Fig. 3. Representative volume element (RVE) with CNTs agglomeration

The entire volume V_r of CNTs contained in the RVE can be split into two portions, which are as follows:

$$V_r = V_r^{inclusion} + V_r^m \quad (23)$$

where

$V_r^{inclusion}$ = volumes of CNT dispersed in the inclusions

V_r^m = volumes of CNT dispersed in the matrix

To understand clearly the effect of carbon nanotube agglomeration, two parameters are introduced as ξ , and ζ .

$$\xi = \frac{V_r^{inclusion}}{V}, \zeta = \frac{V_r^{inclusion}}{V_r} \quad (24)$$

where,

$V_r^{inclusion}$ = volume of the RVE's sphere inclusions.

In this case, ξ represents the volume fraction of inclusions in relation to the RVE's total volume V . Whenever ξ is equal to one, CNTs are assumed to be equally dispersed across the matrix, and as the value of ξ decreases, the degree of agglomeration of carbon nanotubes becomes more severe (Fig. 5). The parameter ζ represents the volume ratio of the CNTs to the overall volume of the nanotubes scattered in inclusions. When the value ζ is 1, it is presumed that all of the CNTs are clustered in spherical regions.

This is true if all nanotubes are dispersed evenly (i.e., $\zeta = \xi$) throughout the matrix. As the value of ζ increases (i.e., $\zeta > \xi$), the CNTs' spatial distribution becomes more. V_{cnt} is an abbreviation that stands for the average CNT volume fraction found in the composite.

$$V_{cnt} = \frac{V_r}{V} \quad (25)$$

The carbon nanotube volume fractions in the inclusions and the matrix are calculated using Eqs. (23)-(25), and they are expressed as

$$\frac{V_r^{inclusion}}{V_r^{inclusion}} = V_{cnt} \frac{\zeta}{\xi} \quad (26)$$

$$\frac{V_r^m}{V - V_r^{inclusion}} = \frac{V_{cnt} (1 - \zeta)}{1 - \xi} \quad (27)$$

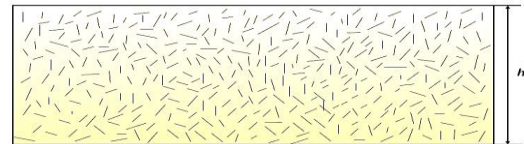


Fig. 4. $\zeta = \xi = 1$ (Without agglomeration) [75]

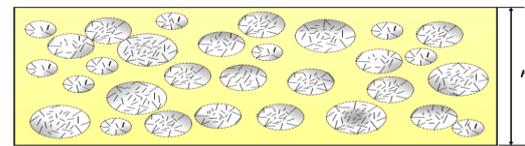


Fig. 5. $\zeta = 1, \xi < \zeta$ (Complete agglomeration) [75]

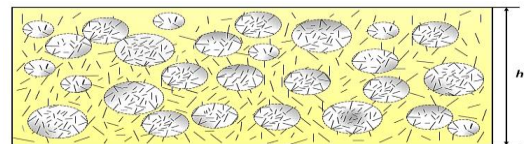


Fig. 6. $\zeta < \xi < \zeta$ (Partial agglomeration) [75]

As a result, the Composite reinforced with carbon nanotubes is viewed as a system made up of sphere-shaped inclusions embedded in a hybrid matrix. CNTs can be found in both the matrix as well as in the inclusions also. Hence to

compute the composite system's overall property first we have to individually estimate the effective elastic properties of both inclusions and matrix respectively.

Different micromechanics methods can be used to calculate the effective modulus of elasticity of the hybrid inclusions and matrix. Assuming that all CNT orientations are completely random, and the nanotubes are transversely isotropic, the Mori-Tanaka method is used to estimate the hybrid matrix's elastic moduli, as stated in the preceding section. It is expected that the carbon nanotubes are arranged in a random manner within the inclusions, and thus the inclusions are isotropic. Where, K_{in} and K_{out} represent the effective bulk moduli, while G_{in} and G_{out} are the effective shear moduli of the inclusions and matrix.

$$K_{in} = K_m + \frac{V_{cnt}\zeta(\delta_r - 3K_m\alpha_r)}{3(\xi - V_{cnt}\zeta + V_{cnt}\zeta\alpha_r)} \quad (28)$$

$$K_{out} = K_m + \frac{V_{cnt}(1-\zeta)(\delta_r - 3K_m\alpha_r)}{[3(1-\xi - V_{cnt}(1-\zeta) + V_{cnt}(1-\zeta)\alpha_r)]} \quad (29)$$

$$G_{in} = G_m + \frac{V_{cnt}\zeta(\eta_r - 2G_m\beta_r)}{2(\xi - V_{cnt}\zeta + V_{cnt}\zeta\beta_r)} \quad (30)$$

$$G_{out} = G_m + \frac{V_{cnt}(1-\zeta)(\eta_r - 2G_m\beta_r)}{[2(1-\xi - V_{cnt}(1-\zeta) + V_{cnt}(1-\zeta)\beta_r)]} \quad (31)$$

Following that, the composite's effective bulk and shear modulus are computed using the method proposed by Mori-Tanaka as follows:

$$K = K_{out} \left[1 + \frac{\xi \left(\frac{K_{in}}{K_{out}} - 1 \right)}{1 + \alpha(1-\xi) \left(\frac{K_{in}}{K_{out}} - 1 \right)} \right] \quad (32)$$

$$G = G_{out} \left[1 + \frac{\xi \left(\frac{G_{in}}{G_{out}} - 1 \right)}{1 + \beta(1-\xi) \left(\frac{G_{in}}{G_{out}} - 1 \right)} \right] \quad (33)$$

where,

$$v_{out} = \left(\frac{3K_{out} - 2G_{out}}{2(3K_{out} + G_{out})} \right), \quad (34)$$

$$\alpha = \frac{(1 + v_{out})}{3(1 - v_{out})}, \quad \beta = \frac{2(4 - 5v_{out})}{15(1 - v_{out})}$$

In the final step, Eq. (16) is used to determine the young's modulus of nanocomposite material.

3. Formulation

3.1. In a plane, strains, and displacement fields

The FGM plate's geometry used in this analysis is shown in Fig. 7. The center of the FG plate serves as the reference point. Plates are simply supported along their four edges, with $a = b$ for the square plate. $a/h=10$ is the aspect ratio taken into account between the x-edge and thickness.

It is possible to make use of the higher-order shear deformation theory proposed by Reddy [50] in order to provide an explanation for in-plane displacement variations of u and v as well as the transverse displacement w throughout the thickness of the plate.

$$u(x, y, z) = u_0 + z\theta_x - \frac{4z^3}{3h^2}\gamma_x$$

$$v(x, y, z) = v_0 + z\theta_y - \frac{4z^3}{3h^2}\gamma_y \quad (35)$$

$$w(x, y) = w_0$$

where

u_0, v_0, w_0 = mid-plane displacements of a point along the (x, y, z) coordinates.

θ_x, θ_y = bending rotations in the x and y directions.

γ_x, γ_y = assumed shear rotations in the x and y directions.

The following definition should be used to describe the relationship between the strain component and the strain displacement:

$$\{\epsilon_m\} = \begin{Bmatrix} \frac{\partial u}{\partial x} \\ \frac{\partial v}{\partial y} \\ \frac{\partial u}{\partial y} + \frac{\partial v}{\partial x} \\ \frac{\partial u}{\partial z} + \frac{\partial w}{\partial x} \\ \frac{\partial v}{\partial z} + \frac{\partial w}{\partial y} \end{Bmatrix} = \begin{Bmatrix} \frac{\partial u_0}{\partial x} + z \frac{\partial \theta_x}{\partial x} - \frac{4z^3}{3h^2} \frac{\partial \gamma_x}{\partial x} \\ \frac{\partial v_0}{\partial y} + z \frac{\partial \theta_y}{\partial y} - \frac{4z^3}{3h^2} \frac{\partial \gamma_y}{\partial y} \\ \frac{\partial u_0}{\partial y} + z \frac{\partial \theta_x}{\partial x} - \frac{4z^3}{3h^2} \frac{\partial \gamma_x}{\partial x} + \frac{\partial v_0}{\partial x} + z \frac{\partial \theta_y}{\partial y} - \frac{4z^3}{3h^2} \frac{\partial \gamma_y}{\partial y} \\ \frac{\partial w_0}{\partial x} + \theta_x - \frac{4z^3}{h^2} \gamma_x \\ \frac{\partial w_0}{\partial y} + \theta_y - \frac{4z^3}{h^2} \gamma_y \end{Bmatrix} \quad (36)$$

The overall strain in terms of mechanical strain, moisture- strain, and thermal strain is as follows:

$$\{\varepsilon\} = \{\varepsilon_m\} + \{\varepsilon_\alpha\} + \{\varepsilon_\beta\} \quad (37)$$

where

- $\{\varepsilon_m\}$ = mechanical strain
- $\{\varepsilon_\alpha\}$ = thermal strain
- $\{\varepsilon_\beta\}$ = moisture strain

Finally, mechanical strain can be expressed in terms of global strain as

$$\{\varepsilon_m\} = [H]\{\varepsilon\} \quad (38)$$

where $\{\varepsilon\}$ is a function of the two dimensions (x,y), and [H] is a function of the third dimension (z). Additionally, thermal stress may be stated as

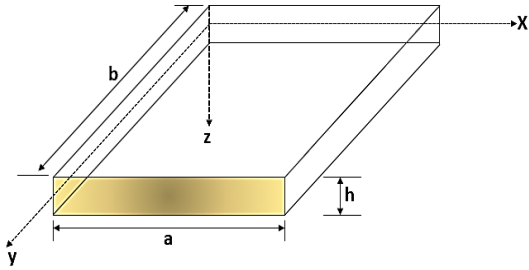


Fig. 7. Geometry of the FGCNT Plate

$$\{\varepsilon_\alpha\} = \int_{-h/2}^{h/2} \begin{Bmatrix} \alpha(z, T) \\ \alpha(z, T) \\ 0 \\ 0 \\ 0 \end{Bmatrix} dz \quad (39)$$

Moisture (i.e., hygro) strain due to moisture change is given by

$$\{\varepsilon_\beta\} = \int_{-h/2}^{h/2} \begin{Bmatrix} \beta(z, C) \\ \beta(z, C) \\ 0 \\ 0 \\ 0 \end{Bmatrix} dz \quad (40)$$

in which ΔT and ΔC are the change of temperature/moisture concentration with respect to reference temperature/moisture concentration.

Hence to combine Eqs. (38), (39), and (40), the total strain can be expressed as,

$$\{\varepsilon\} = [H]\{\varepsilon\} + \{\varepsilon_\alpha\} + \{\varepsilon_\beta\} \quad (41)$$

3.2. Constitutive Relationship

The following is an illustration of the relationship between stress and strain for FGM:

$$\{\sigma\} = [Q]\{\varepsilon\} \quad (42)$$

where, constitutive matrix

$$[Q] = \begin{bmatrix} Q_{11} & Q_{12} & 0 & 0 & 0 \\ Q_{21} & Q_{22} & 0 & 0 & 0 \\ 0 & 0 & Q_{33} & 0 & 0 \\ 0 & 0 & 0 & Q_{44} & 0 \\ 0 & 0 & 0 & 0 & Q_{55} \end{bmatrix} \begin{Bmatrix} \varepsilon_x - \alpha \Delta T - \beta \Delta C \\ \varepsilon_y - \alpha \Delta T - \beta \Delta C \\ \gamma_{xy} \\ \gamma_{xz} \\ \gamma_{yz} \end{Bmatrix} \quad (43)$$

where,

- ΔT = (T-To) = difference of applied and reference temperature.
- ΔC = (C-Co) = difference in moisture concentration to reference moisture concentration.
- α = The coefficient of thermal expansion or contraction owing to temperature.
- β = coefficient of expansion or contraction owing to moisture.

In Eq. (43) the term Q_{ij} are derived from the material properties, depending on the plate's depth(z) as shown below in Eq. (44).

$$\begin{aligned} Q_{11} &= Q_{22} = \frac{E(z)}{1 - \gamma^2} \\ Q_{12} &= Q_{21} = \frac{\gamma E(z)}{1 - \gamma^2} \\ Q_{33} &= Q_{44} = Q_{55} = \frac{E(z)}{2(1 + \gamma)} \end{aligned} \quad (44)$$

3.3. Virtual Work in FGCNT Plate

The FGM plate's virtual work may be expressed as

$$\delta U = \iiint \{\delta\varepsilon\}^T \{\sigma\} dx dy dz \quad (45)$$

The Eq. (45) shown before can be rewritten using the Eq. (42) as follows:

$$\delta U = \iiint \{\delta\varepsilon\}^T [Q]\{\varepsilon\} dx dy dz \quad (46)$$

The following equation can be extended further using Eq. (40) as follows:

$$\delta U = \iiint \{\delta\varepsilon\}^T [H]^T [Q][H]\{\varepsilon\} dx dy dz \quad (47)$$

In Eq. (46) the matrix [Q] represents the constitutive matrix with elasticity derived from the constituent's elastic properties as given in Eq. (43). While [H] represents the 5 x 15 order matrix

and includes the terms z and h as described below:

$$[H] = \begin{bmatrix} 1 & 0 & 0 & 0 & 0 & z & 0 & 0 & 0 & 0 & 0 & 0 & \frac{-4z^3}{3h^2} & 0 & 0 \\ 0 & 1 & 0 & 0 & 0 & 0 & z & 0 & 0 & 0 & 0 & 0 & \frac{-4z^3}{3h^2} & 0 & 0 \\ 0 & 0 & 1 & 0 & 0 & 0 & 0 & z & 0 & 0 & 0 & 0 & 0 & \frac{-4z^3}{3h^2} & 0 \\ 0 & 0 & 0 & 1 & 0 & 0 & 0 & 0 & 1 & 0 & \frac{-4z^2}{h^2} & 0 & 0 & 0 & 0 \\ 0 & 0 & 0 & 0 & 1 & 0 & 0 & 0 & 0 & 1 & 0 & \frac{-4z^2}{h^2} & 0 & 0 & 0 \end{bmatrix} \quad (48)$$

Finally, we can rewrite Eq. (47) as

$$\delta U = \iint \{\delta \varepsilon\}^T [D] \{\varepsilon\} dx dy \quad (49)$$

where matrix $[D]$ represents the rigidity matrix vector. For which the corresponding expression is given in Eq. (50) shown below.

$$[D] = \int_{-\frac{h}{2}}^{\frac{h}{2}} [H]^T [Q] [H] dz \quad (50)$$

4. Finite Element Formulation

4.1. Element Description

Figure 8 illustrates the isoparametric Lagrangian element's geometry with nine nodes used in the analysis. In this element, there is a total of sixty-three degrees of freedom because each node has seven degrees of freedom (u , v , w , θ_x , θ_y , γ_x and γ_y). In the x - y plane co-ordinate system, this element has a rectangular geometry that is completely arbitrary. The element is transferred to the ξ - η plane in order to get a rectangular geometry.

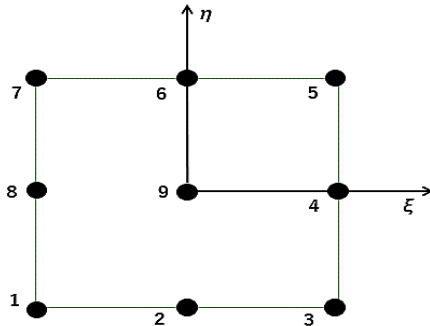


Fig. 8. Nine Node Isoperimetric Element with node numbering

The following shape functions are applied to this nine-node element:

$$\begin{aligned} N_1 &= \frac{1}{4}(\xi - 1)(\eta - 1)\xi\eta, \\ N_2 &= \frac{1}{4}(\xi + 1)(\eta - 1)\xi\eta, \\ N_3 &= \frac{1}{4}(\xi + 1)(\eta + 1)\xi\eta, \\ N_4 &= \frac{1}{4}(\xi - 1)(\eta + 1)\xi\eta, \\ N_5 &= -\frac{1}{2}(1 - \xi^2)(1 - \eta)\eta, \\ N_6 &= \frac{1}{2}(1 + \xi)(\eta^2 - 1)\xi, \\ N_7 &= -\frac{1}{2}(\xi^2 - 1)(\eta + 1)\eta, \\ N_8 &= -\frac{1}{2}(\xi - 1)(\eta^2 - 1)\xi, \\ N_9 &= (1 - \xi^2)(1 - \eta^2) \end{aligned} \quad (51)$$

The nine shape functions listed above can be used to establish a relationship between strain and displacement. The vector of a strain can be expressed in the following way:

$$\{\varepsilon\} = [B]\{X\} \quad (52)$$

The nodal displacement vector for the selected element is represented by matrix $[X]$ in Eq. (52) whereas matrix $[B]$ is known as a strain-displacement matrix having the order 15×7 and involves the derivatives of shape function terms. Both matrices can be expressed as follows:

$$\begin{aligned} [B] &= [B_1 \ B_2 \ B_3 \ B_4 \ B_5 \ B_6 \ B_7 \ B_8 \ B_9] \\ [X] &= [X_1 \ X_2 \ X_3 \ X_4 \ X_5 \ X_6 \ X_7 \ X_8 \ X_9] \end{aligned} \quad (53)$$

4.2. Governing Equations Used for Flexural Analysis

For the static analysis of the FGCNT plate, the following equation provides the governing equation. The variation of the strain vector can be expressed as follows using Eq. (54).

$$\{\delta \varepsilon\} = [B]\{\delta X\} \quad (54)$$

By combining Eqs. (49) and (54), the following expression can be obtained.

$$\delta U = \{\delta X\}^T \left[\left(\iint [B]^T [D] [B] dx dy \right) \{X\} + \left(\iint [B]^T [F_i] dx dy \right) \right] \quad (55)$$

In the following form, the stiffness matrix, denoted by $[K]$, as well as the nodal thermal vector, denoted by $[P_i]$, can be stated by utilizing Eq. 55.

$$[K] = \iint [B]^T [D] [B] dx dy \quad (56)$$

$$\{P_i\} = \iint [B]^T [F_i] dx dy \quad (57)$$

5. Numerical Results & Discussion

In this section, many numerical examples were studied for the hygrothermal behavior of functionally graded nanocomposite plates with different distributions of carbon nanotube (Fig. 1). It has been done by considering various agglomeration stages as shown in Fig. (4)–(6). This section is separated into two distinct sections. The first phase involves a convergence study and validation of the current formulation for isotropic plates [52] with varying aspect ratios, as no solution exists for the current problem. After confirming the effectiveness of the current formulation, the second step investigates the impacts of various agglomeration stages on the nondimensional central deflection of the plate. In all the above phases, here only simply supported boundary conditions with different CNT distributions are investigated considering three stages of agglomeration (Fig. 4) as (without agglomeration case), (complete agglomeration case) and (partial agglomeration case) are investigated.

The properties of SWCNT (10,10) are listed in Table 1. The matrix substance employed in this situation has the following elastic characteristics: $E_m = 2.5 \text{ GPa}$, $\nu_m = 0.3$, $\rho_m = 1150 \text{ kg/m}^3$, and Table 1 lists the material characteristics of the reinforcement. The UD, FG-X, and FG-O type reinforcement distributions with various levels of agglomeration testing were taken into consideration. Here, 7.5% CNT value is taken into consideration, which is a significant number of carbon nanotubes.

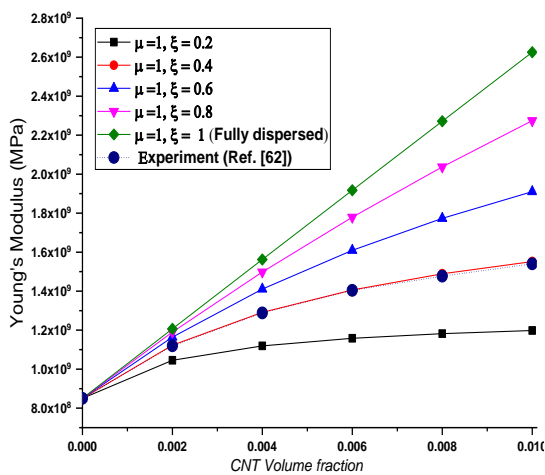


Fig. 9 Young's modulus for various agglomeration levels and CNT volume fractions

First, before the verification and convergence study the mechanical properties were verified with the experimental work done by Odegard et al. [63] and presented in Fig. 9. It is clear, as can be seen by examining Fig. 9, that the Eshelby-Mori-Tanaka scheme proposed by Shi et al. [27]

for the estimation of material properties and the results generated by Odegard et al. [63] are very close for the prediction of mechanical properties. The result produced by the EMT approach for the agglomeration parameter $\xi = 0.4$ corresponding to $\zeta = 1$ (resembles the complete agglomeration behavior) is plotted in Fig. 9 with good agreement. The material for the matrix is used as $E_m = 0.85 \text{ GPa}$ and $\nu_m = 0.3$, combined with the CNT properties given in Table 1 using the EMT approach to calculate overall mechanical properties for the analysis. The results generated here show at the value of parameter $\xi = 1$ the rise in Young's modulus as a function of volume percent is greater than any other modulus. However, as the value of ξ drops, the severity of the agglomeration effect causes an increase in mechanical properties that does not correspond to the expected increase in CNT volume fraction. This is due to the projected increase in mechanical characteristics. Figure 9 itself is self-explanatory and at the highest values of Young's modulus, both agglomeration parameters are considered equal values. Additionally, it is easy to see that the variation of the parameter ξ has a greater effect on mechanical properties than the variation of the other parameter ζ . After a thorough study of the effect of two agglomeration parameters (ζ & ξ) on overall elastic properties, three different stages of agglomeration are generated in the next section to understand the free vibration behavior of square plate with three types of CNT distribution patterns.

The static analysis of a functionally graded nanocomposite plate with varying distributions of carbon nanotubes (shown in Figure 1) has been carried out in this part by taking into account the various stages of agglomeration, which are depicted in Fig. (4) through Fig. (6). This section is separated into two distinct sections. The first phase involves a convergence study and validation of the current formulation for isotropic plates with varying aspect ratios, as no solution exists for the current problem. The conclusion is reported solely for the situation of uniformly distributed thermal load. After confirming the effectiveness of the current formulation, the second step investigates the impacts of various agglomeration stages on the central deflections and axial and transverse stresses of the plate. In all the above phases, only simply supported boundary conditions with different CNT distributions are investigated considering three stages of agglomeration (Fig.4) as $\zeta = \xi = 1$ (without agglomeration case), $\zeta = 1, \xi < \zeta$ (complete agglomeration case) and $\zeta < \xi, \xi < \zeta$ (partial agglomeration case) are investigated. The properties of SWCNT (10,10) are listed in

Table 1. The matrix material used as $E_m = 2.1$ GPa, $\nu_m = 0.34$. A value of $v_{cnt}^* = 0.075$ is considered with a concentration value of 7.5 %, which is a large number of carbon nanotubes [64].

Table 1. CNTRC material properties [51]

Material	P (kg/m ³)	E (GPa)	$\beta(10^{-4}/K)$	$\alpha(10^{-6}/K)$	K (GPa)	G (GPa)
PMMA	1150	2.5	20	45	2.6	0.93
CNT	1400	5646.6	3	3.45	-	-

5.1. Validation:

The isotropic plate has dimensions as $a = b$. The coordinate system's origins ($x, y,$ and z) are set to the plate's mid-plane (i.e., $z = 0$). For isotropic plates having $E = 210$ GPa, $\nu = 0.3$, and $\alpha_x = \alpha_y$ the Convergence study and with shown in Table 2. Several thickness ratios (h/a) are evaluated assuming the edges are simply supported. According to the results of the convergence investigation, a 16×16 mesh is sufficient for thermal analysis when using the current isoparametric Lagrangian element with nine nodes. As a result, for all subsequent examples involving agglomerated functionally graded plates, a 16×16 mesh is used. The non-dimensional parameters for deflection at the centre point considered are: $\bar{w} = w / \alpha_x T_0 b^3 h$.

The results are compared to those of Shinde et al., which are based on the hyperbolic shear deformation theory and investigated using the FE method. For various plate ratios (h/a) as 0.2, 0.1, and 0.05, the present results are compared, and very close agreements are noted between the results obtained from the two approaches.

After verification of the present model, the primary goal of this research was to see the effect of agglomeration with various CNT distributions (Fig. 1) on a deflection at the center point of the simply supported square plate, which is presented in the next section.

5.2. Flexural Response of Simply Supported Square Plate under Various Combinations of Hygrothermal Environments

In the current study, the flexural behavior of a square plate under a hygrothermal environment having simply supported boundary condition (Fig. 7) is evaluated using the nine-noded isoparametric Lagrangian element with 16×16 mesh division with various agglomeration schemes namely, (i). square plate without agglomeration effect ($\xi = \zeta = 1$), (ii). Square plate with complete agglomeration effect ($\zeta = 1, \xi < \zeta$), (iii) square plate with partial agglomeration effect ($\zeta < \xi, \xi < \zeta$). To study the flexural behavior of three types of CNT distributions through the thickness, various values of ζ & ξ are taken, and the results are plotted for non-dimensional central deflections in Fig. 10-15. To understand the behavior for the complete agglomeration stage corresponding to other higher values of ζ it is observed that when $\xi = 0.15$ is verified from $\zeta = 1$, a greater degree of agglomeration occurs.

5.2.1 New Results for Agglomerated FG-CNTRs Square Plate under Hygrothermal Environment

agglomerated CNT-reinforced functionally graded plate results from the increased limitations at the boundary. Since the present study is based on the agglomeration effect of CNT, it can be seen through the result given in Table (3)-(8) for three stages of CNT agglomeration by varying the two-agglomeration parameters ζ & ξ . Figures (10)-(15) show how the non-dimensional central deflection of the nanocomposite plate is affected by the temperature, the amount of moisture, and the combination of both. It has been shown that the central deflection rises when either the temperature or the moisture concentration increases, and it also increases when both of these variables increase simultaneously. When simply the influence of moisture is examined, the rise is at its smallest, but it is greatest when thermal conditions are taken into account.

Table 2. A Comparison of the transverse displacements \bar{w} of a square isotropic plate with different aspect ratios when it is subjected to a uniformly distributed thermal load.

No of Element	Reference [52] (h/a =0.2)	Present (h/a=0.2)	Refer [52] (h/a =0.1)	Present (h/a=0.1)	Reference [52] (h/a =0.05)	Present (h/a=0.05)
2 x 2	-	0.4505	-	0.7880	-	1.0505
4 x 4	-	0.4771	-	0.9465	-	1.8329
6 x 6	-	0.4785	-	0.9555	-	1.8988
8 x 8	-	0.4787	-	0.9570	-	1.9102
10 x 10	-	0.4788	-	0.9574	-	1.9133
12 x 12	-	0.4788	-	0.9575	-	1.9144
14 x 14	-	0.4788	-	0.9576	-	1.9149
16 x 16	0.4789	0.4788	0.9579	0.9576	1.9157	1.9151

5.2.2 Hygro-thermal Analysis without Agglomeration Effect

(3) is for without agglomeration effect of CNT with simply supported boundary conditions and various aspect ratios.

In this section agglomeration effect of CNT is not considered ($\zeta=\xi$). The result presented in Table

Table 3. Comparison of the central deflection \bar{W} for the simply supported rectangular FG plates under three different combinations of hygrothermal loading with various aspect ratios along with varying CNT percentage (Without Agglomeration Effect):

CNT Pattern	b/h	SSSS	SSSS	SSSS
		$\Delta T = 0, \Delta C = 10\%$	$\Delta T = 100, \Delta C = 0\%$	$\Delta T = 100, \Delta C = 10\%$
$v_{cnt}^*=0.05, \zeta=0.25, \xi=0.25$				
UD	2	1.03E-03	1.24E-04	1.15E-03
	5	6.41E-03	7.73E-04	7.18E-03
	10	2.56E-02	3.09E-03	2.87E-02
	20	1.03E-01	1.24E-02	1.15E-01
FG-X	2	1.01E-03	1.20E-04	1.13E-03
	5	6.33E-03	7.53E-04	7.08E-03
	10	2.53E-02	3.01E-03	2.83E-02
	20	1.01E-01	1.21E-02	1.13E-01
FG-O	2	1.08E-03	1.36E-04	1.21E-03
	5	6.71E-03	8.48E-04	7.55E-03
	10	2.68E-02	3.39E-03	3.02E-02
	20	1.07E-01	1.35E-02	1.21E-01
$v_{cnt}^*=0.075, \zeta=0.25, \xi=0.25$				
UD	2	1.01E-03	1.20E-04	1.13E-03
	5	6.33E-03	7.53E-04	7.08E-03
	10	2.53E-02	3.01E-03	2.83E-02
	20	1.01E-01	1.20E-02	1.13E-01
FG-X	2	1.00E-03	1.18E-04	1.12E-03
	5	6.28E-03	7.39E-04	7.02E-03
	10	2.51E-02	2.96E-03	2.81E-02
	20	1.00E-01	1.18E-02	1.12E-01
FG-O	2	1.04E-03	1.28E-04	1.17E-03
	5	6.51E-03	7.99E-04	7.31E-03
	10	2.60E-02	3.19E-03	2.92E-02
	20	1.04E-01	1.28E-02	1.17E-01
$v_{cnt}^*=0.1, \zeta=0.25, \xi=0.25$				
UD	2	1.01E-03	1.19E-04	1.13E-03
	5	6.29E-03	7.42E-04	7.03E-03
	10	2.52E-02	2.97E-03	2.81E-02
	20	1.01E-01	1.19E-02	1.12E-01
FG-X	2	9.99E-04	1.17E-04	1.12E-03
	5	6.25E-03	7.32E-04	6.98E-03
	10	2.50E-02	2.93E-03	2.79E-02
	20	1.00E-01	1.17E-02	1.12E-01
FG-O	2	1.03E-03	1.24E-04	1.15E-03
	5	6.42E-03	7.76E-04	7.20E-03
	10	2.57E-02	3.10E-03	2.88E-02
	20	1.03E-01	1.24E-02	1.15E-01
$v_{cnt}^*=0.2, \zeta=0.25, \xi=0.25$				
UD	2	9.97E-04	1.16E-04	1.11E-03
	5	6.23E-03	7.27E-04	6.96E-03
	10	2.49E-02	2.91E-03	2.78E-02
	20	9.97E-02	1.16E-02	1.11E-01
FG-X	2	9.93E-04	1.15E-04	1.11E-03
	5	6.21E-03	7.22E-04	6.93E-03
	10	2.48E-02	2.89E-03	2.77E-02
	20	9.94E-02	1.16E-02	1.11E-01
FG-O	2	1.01E-03	1.19E-04	1.13E-03
	5	6.29E-03	7.42E-04	7.03E-03
	10	2.51E-02	2.97E-03	2.81E-02
	20	1.01E-01	1.19E-02	1.12E-01
$v_{cnt}^*=0.3, \zeta=0.25, \xi=0.25$				
UD	2	9.94E-04	1.16E-04	1.11E-03
	5	6.21E-03	7.22E-04	6.93E-03
	10	2.48E-02	2.89E-03	2.77E-02
	20	9.94E-02	1.16E-02	1.11E-01
FG-X	2	9.92E-04	1.15E-04	1.11E-03
	5	6.20E-03	7.19E-04	6.92E-03
	10	2.48E-02	2.88E-03	2.77E-02
	20	9.92E-02	1.15E-02	1.11E-01

FG-O	2	1.00E-03	1.17E-04	1.12E-03
	5	6.24E-03	7.31E-04	6.98E-03
	10	2.50E-02	2.92E-03	2.79E-02
	20	9.99E-02	1.17E-02	1.12E-01
$v_{cnt}^*=0.4 \zeta=0.25, \xi=0.25$				
UD	2	9.92E-04	1.15E-04	1.11E-03
	5	6.20E-03	7.20E-04	6.92E-03
	10	2.48E-02	2.88E-03	2.77E-02
	20	9.92E-02	1.15E-02	1.11E-01
FG-X	2	9.91E-04	1.15E-04	5.00E+00
	5	6.19E-03	7.17E-04	6.91E-03
	10	2.48E-02	2.87E-03	2.76E-02
	20	9.91E-02	1.15E-02	1.11E-01
FG-O	2	9.96E-04	1.16E-04	1.11E-03
	5	6.22E-03	7.25E-04	6.95E-03
	10	2.49E-02	2.90E-03	2.78E-02
	20	9.95E-02	1.16E-02	1.11E-01
$v_{cnt}^*=0.5 \zeta=0.25, \xi=0.25$				
UD	2	9.92E-04	1.15E-04	1.11E-03
	5	6.20E-03	7.18E-04	6.92E-03
	10	2.48E-02	2.87E-03	2.77E-02
	20	9.92E-02	1.15E-02	1.11E-01
FG-X	2	9.91E-04	1.15E-04	1.11E-03
	5	6.19E-03	7.16E-04	6.91E-03
	10	2.48E-02	2.87E-03	2.76E-02
	20	9.91E-02	1.15E-02	1.11E-01
FG-O	2	9.94E-04	1.16E-04	1.11E-03
	5	6.21E-03	7.22E-04	6.93E-03
	10	2.48E-02	2.89E-03	2.77E-02
	20	9.94E-02	1.15E-02	1.11E-01

5.2.3 Hygro-thermal Analysis under Complete Agglomeration Effect

This section discusses the complete agglomeration effect, which is based on the assumption that all of the CNTs have accumulated in the inclusion that has a spherical shape. Here, in this section three types of combinations for ζ & ξ are considered for the analysis of this particular agglomeration stage. As we can see from Table (6) – (8) as the parameter ξ increases from 0.15 to 0.75 corresponding to $\zeta=1$, the stage where ξ is equal to 0.15 means all CNTs are presented in the matrix as circular clusters have less stiffness as compared to $\xi = 0.75$ stage. The stage $\zeta=1$ and $\xi= 0.15$ represents the worst case of the agglomeration stage. Next, as the value of ξ reaches towards ζ the CNTs which are present in stage 1 in a cluster will try to free from cluster effect by uniform mixing with the surrounding matrix. Overall, from Table (6) to Table (8) it can easily be understood that case 3 where $\zeta=1$ and $\xi= 0.75$ shows a higher value of nondimensional central deflection as compared to the other two stages under complete agglomeration effect.

According to the findings of the study, the elasticity of the material would be impacted more by the agglomeration of carbon nanotubes in proportion to the degree to which the values of the agglomeration parameters differed from one another. The same explanation can also be understood by glancing at the illustration that is labeled Fig. (9). The difference in the nondimensional central deflection is quite significant when contrasted with the responses of

other cases of complete agglomeration. The difference between the two groups of findings is rather substantial when measured against the flexural response that was acquired in the section before this one without the agglomeration stage. Table (4)-(6) shows the nondimensional central deflections for three different cases of complete agglomeration, taking into account the three distinct CNT dispersion patterns along the direction of the plate's thickness. From the table, we can see that in all instances of total agglomeration, the FG-O has the worst hygrothermal flexural behavior compared with relation to the other CNT distributions that are now in the same condition of total agglomeration.

When taken as a whole, it is possible to state that, for a stage that has been entirely agglomerated, the three CNT distributions that are being investigated will have lower central deflection if the distribution is more heterogeneous. It is possible to arrive at the conclusion that the FG-X distribution demonstrates superior hygrothermal behavior in addition to the level of agglomeration because CNTs are distributed in regions with higher bending stress.

From Table (4)-(5) it could be understood that as ξ increases the flexural response under hygrothermal environment shows a higher value which shows that the agglomeration or clustering of CNT has a beneficial effect as represented in Fig. (18)-(22). Table 4 which is for the worst case of agglomeration (Case-1) shows a lesser value as compared to other higher values of ξ .

5.2.4 Hygro-thermal Analysis under Partial Agglomeration Effect

Similarly, we can conclude the partial agglomeration effect in which some CNTs are present in cluster form and some CNTs are present in the matrix. In this partial agglomeration stage, two types of agglomeration stages were considered for the study in which ζ & ξ will have two different values to create a partial agglomeration stage. In the first stage where $\zeta =$

0.25 and $\xi = 0.4$ by assuming the maximum number of CNTs are present in the cluster form some CNTs will present in the matrix, while in the second stage, $\zeta = 0.75$ and $\xi = 0.4$ is used to show that maximum number of CNTs are present in matrix and only little percentage of CNTs are forming clusters of CNT. Comparing both stages reveals that their behavior with respect to nondimensional central deflection is nearly identical.

Table 4. Comparison of the central deflection \bar{W} for the simply supported rectangular FG plates under three different combinations of hygrothermal loading with various aspect ratios along with varying CNT percentage (Complete Agglomeration Case-1):

CNT Pattern	b/h	SSSS	SSSS	SSSS
		$\Delta T = 0, \Delta C = 10\%$	$\Delta T = 100, \Delta C = 0\%$	$\Delta T = 100, \Delta C = 10\%$
$v_{cnt}^* = 0.05, \zeta = 1, \xi = 0.15$				
UD	2	1.01E-03	1.22E-04	1.13E-03
	5	6.31E-03	7.61E-04	7.07 E-03
	10	2.52E-02	3.04E-03	2.83E-02
	20	1.01E-01	1.22E-02	1.13E-01
FG-X	2	9.99E-04	1.19E-04	1.12 E-03
	5	6.25E-03	7.47E-04	7.00 E-03
	10	2.50E-02	2.99E-03	2.80E-02
	20	1.00E-01	1.20E-02	1.12E-01
FG-O	2	1.09E-03	1.42E-04	1.23E-03
	5	6.79E-03	8.79E-04	7.67E-03
	10	2.72E-02	3.51E-03	3.07 E-02
	20	1.09E-01	1.40E-02	1.23E-01
$v_{cnt}^* = 0.075, \zeta = 1, \xi = 0.15$				
UD	2	9.96E-04	1.18E-04	1.11E-03
	5	6.23E-03	7.40E-04	6.97 E-03
	10	2.49E-02	2.96E-03	2.79 E-02
	20	9.96E-02	1.18E-02	1.11E-01
FG-X	2	9.89E-04	1.17E-04	1.11E-03
	5	6.19E-03	7.31E-04	6.92E-03
	10	2.47E-02	2.92E-03	2.77E-02
	20	9.90E-02	1.17E-02	1.11E-01
FG-O	2	1.05E-03	1.32E-04	1.18E-03
	5	6.55E-03	8.20E-04	7.37E-03
	10	2.62E-02	3.28E-03	2.95E-02
	20	1.05E-01	1.31E-02	1.18E-01
$v_{cnt}^* = 0.1, \zeta = 1, \xi = 0.15$				
UD	2	9.89E-04	1.17E-04	1.11E-03
	5	6.18E-03	7.30E-04	6.91E-03
	10	2.47E-02	2.92E-03	2.77E-02
	20	9.89E-02	1.17E-02	1.11E-01
FG-X	2	9.84E-04	1.15E-04	1.10E-03
	5	6.15E-03	7.23E-04	6.88E-03
	10	2.46E-02	2.89E-03	2.75E-02
	20	9.85E-02	1.16E-02	1.10E-01
FG-O	2	1.03E-03	1.27E-04	1.16E-03
	5	6.43E-03	7.90E-04	7.22E-03
	10	2.57E-02	3.16E-03	2.89E-02
	20	1.03E-01	1.26E-02	1.15E-01

$v_{cnt}^*=0.2, \zeta=1, \xi=0.15$				
UD	2	9.79E-04	1.14E-04	1.09E-03
	5	6.12E-03	7.14E-04	6.83E-03
	10	2.45E-02	2.86E-03	2.73E-02
	20	9.79E-02	1.14E-02	1.09E-01
FG-X	2	9.76E-04	1.14E-04	1.09E-03
	5	6.10E-03	7.11E-04	6.82E-03
	10	2.44E-02	2.84E-03	2.73E-02
	20	9.77E-02	1.14E-02	1.09E-01
FG-O	2	1.00E-03	1.19E-04	1.12E-03
	5	6.24E-03	7.45E-04	6.99E-03
	10	2.50E-02	2.98E-03	2.80E-02
	20	9.99E-02	1.19E-02	1.12E-01
$v_{cnt}^*=0.3, \zeta=1, \xi=0.15$				
UD	2	9.76E-04	1.13E-04	1.09E-03
	5	6.10E-03	7.09E-04	6.81E-03
	10	2.44E-02	2.84E-03	2.72E-02
	20	9.76E-02	1.13E-02	1.09E-01
FG-X	2	9.74E-04	1.13E-04	1.09E-03
	5	6.09E-03	7.07E-04	6.79E-03
	10	2.44E-02	2.83E-03	2.72E-02
	20	9.74E-02	1.13E-02	1.09E-01
FG-O	2	9.90E-04	1.17E-04	1.11E-03
	5	6.18E-03	7.29E-04	6.91E-03
	10	2.47E-02	2.92E-03	2.76E-02
	20	9.89E-02	1.17E-02	1.11E-01
$v_{cnt}^*=0.4, \zeta=1, \xi=0.15$				
UD	2	9.74E-04	1.13E-04	1.09E-03
	5	6.09E-03	7.06E-04	6.79E-03
	10	2.43E-02	2.83E-03	2.72E-02
	20	9.74E-02	1.13E-02	1.09E-01
FG-X	2	9.73E-04	1.13E-04	1.09E-03
	5	6.08E-03	7.05E-04	6.78E-03
	10	2.43E-02	2.82E-03	2.71E-02
	20	9.73E-02	1.13E-02	1.09E-01
FG-O	2	9.85E-04	1.16E-04	1.10E-03
	5	6.15E-03	7.22E-04	6.87E-03
	10	2.46E-02	2.89E-03	2.75E-02
	20	9.84E-02	1.15E-02	1.10E-01
$v_{cnt}^*=0.5, \zeta=1, \xi=0.15$				
UD	2	9.73E-04	1.13E-04	1.09E-03
	5	6.08E-03	7.05E-04	6.79E-03
	10	2.43E-02	2.82E-03	2.71E-02
	20	9.73E-02	1.13E-02	1.09E-01
FG-X	2	9.72E-04	1.13E-04	1.08E-03
	5	6.08E-03	7.03E-04	6.78E-03
	10	2.43E-02	2.81E-03	2.71E-02
	20	9.72E-02	1.13E-02	1.08E-01
FG-O	2	9.81E-04	1.15E-04	1.10E-03
	5	6.13E-03	7.17E-04	6.85E-03
	10	2.45E-02	2.87E-03	2.74E-02
	20	9.81E-02	1.15E-02	1.10E-01

Table 5. Comparison of the central deflection \bar{W} for the simply supported rectangular FG plates under three different combinations of hygrothermal loading with various aspect ratios along with varying CNT percentage (Complete Agglomeration Case-2):

CNT Pattern	a/h	SSSS	SSSS	SSSS
		$\Delta T = 0, \Delta C = 10\%$	$\Delta T = 100, \Delta C = 0\%$	$\Delta T = 100, \Delta C = 10\%$
$v_{cnt}^* = 0.05, \zeta = 1, \xi = 0.45$				
UD	2	1.02E-03	1.23E-04	1.14E-03
	5	6.35E-03	7.66E-04	7.12E-03
	10	2.54E-02	3.06E-03	2.85E-02
	20	1.02E-01	1.23E-02	1.14E-01
FG-X	2	1.01E-03	1.20E-04	1.13E-03
	5	6.29E-03	7.51E-04	7.04E-03
	10	2.52E-02	3.00E-03	2.82E-02
	20	1.01E-01	1.20E-02	1.13E-01
FG-O	2	1.09E-03	1.41E-04	1.23E-03
	5	6.80E-03	8.75E-04	7.67E-03
	10	2.72E-02	3.50E-03	3.07E-02
	20	1.09E-01	1.40E-02	1.23E-01
$v_{cnt}^* = 0.075, \zeta = 1, \xi = 0.45$				
UD	2	1.00E-03	1.19E-04	1.12E-03
	5	6.27E-03	7.45E-04	7.02E-03
	10	2.51E-02	2.98E-03	2.81E-02
	20	1.00E-01	1.19E-02	1.12E-01
FG-X	2	9.96E-04	1.17E-04	1.11E-03
	5	6.23E-03	7.35E-04	6.96E-03
	10	2.49E-02	2.94E-03	2.79E-02
	20	9.97E-02	1.18E-02	1.11E-01
FG-O	2	1.05E-03	1.32E-04	1.19E-03
	5	6.57E-03	8.20E-04	7.39E-03
	10	2.63E-02	3.28E-03	2.96E-02
	20	1.05E-01	1.31E-02	1.18E-01
$v_{cnt}^* = 0.1, \zeta = 1, \xi = 0.45$				
UD	2	9.96E-04	1.18E-04	1.11E-03
	5	6.23E-03	7.35E-04	6.96E-03
	10	2.49E-02	2.94E-03	2.78E-02
	20	9.96E-02	1.18E-02	1.11E-01
FG-X	2	9.91E-04	1.16E-04	1.11E-03
	5	6.20E-03	7.28E-04	6.92E-03
	10	2.48E-02	2.91E-03	2.77E-02
	20	9.92E-02	1.16E-02	1.11E-01
FG-O	2	1.04E-03	1.27E-04	1.16E-03
	5	6.46E-03	7.92E-04	7.25E-03
	10	2.58E-02	3.17E-03	2.90E-02
	20	1.03E-01	1.27E-02	1.16E-01
$v_{cnt}^* = 0.2, \zeta = 1, \xi = 0.45$				
UD	2	9.86E-04	1.15E-04	1.10E-03
	5	6.16E-03	7.19E-04	6.88E-03
	10	2.47E-02	2.88E-03	2.75E-02
	20	9.86E-02	1.15E-02	1.10E-01
FG-X	2	9.84E-04	1.14E-04	1.10E-03
	5	6.15E-03	7.16E-04	6.86E-03
	10	2.46E-02	2.86E-03	2.75E-02
	20	9.84E-02	1.15E-02	1.10E-01
FG-O	2	1.01E-03	1.20E-04	1.13E-03
	5	6.28E-03	7.49E-04	7.03E-03
	10	2.51E-02	3.00E-03	2.81E-02
	20	1.01E-01	1.20E-02	1.12E-01
$v_{cnt}^* = 0.3, \zeta = 1, \xi = 0.45$				
UD	2	9.83E-04	1.14E-04	1.10E-03
	5	6.14E-03	7.14E-04	6.86E-03

	10	2.46E-02	2.86E-03	2.74E-02
	20	9.83E-02	1.14E-02	1.10E-01
FG-X	2	9.81E-04	1.14E-04	1.09E-03
	5	6.13E-03	7.12E-04	6.84E-03
	10	2.45E-02	2.85E-03	2.74E-02
	20	9.81E-02	1.14E-02	1.10E-01
	2	9.97E-04	1.18E-04	1.11E-03
FG-O	5	6.22E-03	7.34E-04	6.96E-03
	10	2.49E-02	2.94E-03	2.78E-02
	20	9.96E-02	1.17E-02	1.11E-01
	$v_{cnt}^*=0.4, \zeta=1, \xi=0.45$			
UD	2	9.81E-04	1.14E-04	1.09E-03
	5	6.13E-03	7.12E-04	6.84E-03
	10	2.45E-02	2.85E-03	2.74E-02
	20	9.81E-02	1.14E-02	1.09E-01
FG-X	2	9.80E-04	1.14E-04	1.09E-03
	5	6.12E-03	7.10E-04	6.83E-03
	10	2.45E-02	2.84E-03	2.73E-02
	20	9.80E-02	1.14E-02	1.09E-01
FG-O	2	9.92E-04	1.16E-04	1.11E-03
	5	6.19E-03	7.27E-04	6.92E-03
	10	2.48E-02	2.91E-03	2.77E-02
	20	9.91E-02	1.16E-02	1.11E-01
$v_{cnt}^*=0.5, \zeta=1, \xi=0.45$				
UD	2	9.80E-04	1.14E-04	1.09E-03
	5	6.13E-03	7.10E-04	6.84E-03
	10	2.45E-02	2.84E-03	2.73E-02
	20	9.80E-02	1.14E-02	1.09E-01
FG-X	2	9.79E-04	1.13E-04	1.09E-03
	5	6.12E-03	7.09E-04	6.83E-03
	10	2.45E-02	2.83E-03	2.73E-02
	20	9.79E-02	1.13E-02	1.09E-01
FG-O	2	9.88E-04	1.16E-04	1.10E-03
	5	6.18E-03	7.22E-04	6.90E-03
	10	2.47E-02	2.89E-03	2.76E-02
	20	9.79E-04	1.13E-04	1.09E-03

Table 6. Comparison of the central deflection \bar{W} for the simply supported rectangular FG plates under three different combinations of hygrothermal loading with various aspect ratios along with varying CNT percentage (Complete Agglomeration Case-3):

CNT Pattern	b/h	SSSS	SSSS	SSSS
		$\Delta T = 0, \Delta C = 10\%$	$\Delta T = 100, \Delta C = 0\%$	$\Delta T = 100, \Delta C = 10\%$
$v_{cnt}^*=0.05, \zeta=1, \xi=0.75$				
UD	2	1.02E-03	1.23E-04	1.14E-03
	5	6.38E-03	7.70E-04	7.15E-03
	10	2.55E-02	3.08E-03	2.86E-02
	20	1.02E-01	1.23E-02	1.14E-01
FG-X	2	1.01E-03	1.20E-04	1.13E-03
	5	6.32E-03	7.53E-04	7.07E-03
	10	2.53E-02	3.01E-03	2.83E-02
	20	1.01E-03	1.20E-02	1.13E-01
FG-O	2	1.08E-03	1.39E-04	1.22E-03
	5	6.76E-03	8.64E-04	7.62E-03
	10	2.70E-02	3.45E-03	3.05E-02
	20	1.08E-01	1.38E-02	1.22E-01
$v_{cnt}^*=0.075, \zeta=1, \xi=0.75$				
UD	2	1.01E-03	1.20E-04	1.13E-03
	5	6.30E-03	7.49E-04	7.05E-03
	10	2.52E-02	3.00E-03	2.82E-02
	20	1.01E-01	1.20E-02	1.13E-01
FG-X	2	1.00E-03	1.18E-04	1.12E-03
	5	6.26E-03	7.38E-04	6.99E-03
	10	2.50E-02	2.95E-03	2.80E-02
	20	1.00E-01	1.18E-02	1.12E-01

	2	1.05E-03	1.31E-04	1.18E-03
FG-O	5	6.56E-03	8.13E-04	7.37E-03
	10	2.62E-02	3.25E-03	2.95E-02
	20	1.05E-01	1.30E-02	1.18E-01
	$v_{cnt}^*=0.1, \zeta=1, \xi=0.75$			
UD	2	1.00E-03	1.18E-04	1.12E-03
	5	6.26E-03	7.39E-04	7.00E-03
	10	2.50E-02	2.96E-03	2.80E-02
	20	1.00E-01	1.18E-02	1.12E-01
FG-X	2	9.95E-04	1.17E-04	1.11E-03
	5	6.23E-03	7.30E-04	6.96E-03
	10	2.49E-02	2.92E-03	2.78E-02
	20	9.96E-02	1.17E-02	1.11E-01
FG-O	2	1.03E-03	1.27E-04	1.16E-03
	5	6.46E-03	7.88E-04	7.25E-03
	10	2.58E-02	3.15E-03	2.90E-02
	20	1.03E-01	1.26E-02	1.16E-01
$v_{cnt}^*=0.2, \zeta=1, \xi=0.75$				
UD	2	9.91E-04	1.16E-04	1.11E-03
	5	6.20E-03	7.23E-04	6.92E-03
	10	2.48E-02	2.89E-03	2.77E-02
	20	9.91E-02	1.16E-02	1.11E-01
FG-X	2	9.88E-04	1.15E-04	1.10E-03
	5	6.18E-03	7.19E-04	6.90E-03
	10	2.47E-02	2.88E-03	2.76E-02
	20	9.88E-02	1.15E-02	1.10E-01
FG-O	2	1.01E-03	1.20E-04	1.13E-03
	5	6.30E-03	7.50E-04	7.05E-03
	10	2.52E-02	3.00E-03	2.82E-02
	20	1.01E-01	1.20E-02	1.13E-01
$v_{cnt}^*=0.3, \zeta=1, \xi=0.75$				
UD	2	9.88E-04	1.15E-04	1.10E-03
	5	6.17E-03	7.18E-04	6.89E-03
	10	2.47E-02	2.87E-03	2.76E-02
	20	9.88E-02	1.15E-02	1.10E-01
FG-X	2	9.86E-04	1.14E-04	1.10E-03
	5	6.16E-03	7.15E-04	6.88E-03
	10	2.46E-02	2.86E-03	2.75E-02
	20	9.86E-02	1.14E-02	1.10E-01
FG-O	2	1.00E-03	1.18E-04	1.12E-03
	5	6.25E-03	7.36E-04	6.99E-03
	10	2.50E-02	2.94E-03	2.79E-02
	20	1.00E-01	1.18E-02	1.12E-01
$v_{cnt}^*=0.4, \zeta=1, \xi=0.75$				
UD	2	9.86E-04	1.14E-04	1.10E-03
	5	6.16E-03	7.15E-04	6.88E-03
	10	2.46E-02	2.86E-03	2.75E-02
	20	9.86E-02	1.14E-02	1.10E-01
FG-X	2	9.84E-04	1.14E-04	1.10E-03
	5	6.15E-03	7.13E-04	6.87E-03
	10	2.46E-02	2.85E-03	2.75E-02
	20	9.84E-02	1.14E-02	1.10E-01
FG-O	2	9.96E-04	1.17E-04	1.11E-03
	5	6.22E-03	7.29E-04	6.95E-03
	10	2.49E-02	2.92E-03	2.78E-02
	20	9.95E-02	1.17E-02	1.11E-01
$v_{cnt}^*=0.5, \zeta=1, \xi=0.75$				
UD	2	9.85E-04	1.14E-04	1.10E-03
	5	6.16E-03	7.13E-04	6.87E-03
	10	2.46E-02	2.85E-03	2.75E-02
	20	9.85E-02	1.14E-02	1.10E-01
FG-X	2	9.84E-04	1.14E-04	1.10E-03
	5	6.15E-03	7.12E-04	6.86E-03
	10	2.46E-02	2.85E-03	2.74E-02
	20	9.84E-02	1.14E-02	1.10E-01
FG-O	2	9.93E-04	1.16E-04	1.11E-03
	5	6.20E-03	7.25E-04	6.93E-03
	10	2.48E-02	2.90E-03	2.77E-02
	20	9.92E-02	1.16E-02	1.11E-01

Table 7. Comparison of the central deflection \bar{W} for the simply supported rectangular FG plates under three different combinations of hygrothermal loading with various aspect ratios along with varying CNT percentage (Partial Agglomeration Case-1):

CNT Pattern	b/h	SSSS	SSSS	SSSS
		$\Delta T = 0, \Delta C = 10\%$	$\Delta T = 100, \Delta C = 0\%$	$\Delta T = 100, \Delta C = 10\%$
$v_{cnt}^* = 0.05, \zeta = 0.25, \xi = 0.4$				
UD	2	1.03E-03	1.24E-04	1.15E-03
	5	6.41E-03	7.73E-04	7.18E-03
	10	2.56E-02	3.09E-03	2.87E-02
	20	1.03E-01	1.24E-02	1.15E-01
FG-X	2	1.01E-03	1.20E-04	1.13E-03
	5	6.33E-03	7.53E-04	7.09E-03
	10	2.53E-02	3.01E-03	2.83E-02
	20	1.01E-01	1.21E-02	1.13E-01
FG-O	2	1.08E-03	1.36E-04	1.21E-03
	5	6.71E-03	8.49E-04	7.56E-03
	10	2.68E-02	3.39E-03	3.02E-02
	20	1.07E-01	1.36E-02	1.21E-01
$v_{cnt}^* = 0.075, \zeta = 0.25, \xi = 0.4$				
UD	2	1.01E-03	1.20E-04	1.13E-03
	5	6.33E-03	7.53E-04	7.08E-03
	10	2.53E-02	3.01E-03	2.83E-02
	20	1.01E-01	1.20E-02	1.13E-01
FG-X	2	1.00E-03	1.18E-04	1.12E-03
	5	6.28E-03	7.39E-04	7.02E-03
	10	2.51E-02	2.96E-03	2.81E-02
	20	1.00E-01	1.18E-02	1.12E-01
FG-O	2	1.04E-03	1.28E-04	1.17E-03
	5	6.51E-03	8.00E-04	7.31E-03
	10	2.61E-02	3.20E-03	2.92E-02
	20	1.04E-01	1.28E-02	1.17E-01
$v_{cnt}^* = 0.1, \zeta = 0.25, \xi = 0.4$				
UD	2	1.01E-03	1.19E-04	1.13E-03
	5	6.29E-03	7.42E-04	7.03E-03
	10	2.52E-02	2.97E-03	2.81E-02
	20	1.01E-01	1.19E-02	1.13E-01
FG-X	2	9.99E-04	1.17E-04	1.12E-03
	5	6.25E-03	7.32E-04	6.98E-03
	10	2.50E-02	2.93E-03	2.79E-02
	20	1.00E-01	1.17E-02	1.12E-01
FG-O	2	1.03E-03	1.24E-04	1.15E-03
	5	6.42E-03	7.76E-04	7.20E-03
	10	2.57E-02	3.10E-03	2.88E-02
	20	1.03E-01	1.24E-02	1.15E-01
$v_{cnt}^* = 0.2, \zeta = 0.25, \xi = 0.4$				
UD	2	9.97E-04	1.16E-04	1.11E-03
	5	6.23E-03	7.27E-04	6.96E-03
	10	2.49E-02	2.91E-03	2.78E-02
	20	9.97E-02	1.16E-02	1.11E-01
FG-X	2	9.94E-04	1.15E-04	1.11E-03
	5	6.21E-03	7.22E-04	6.93E-03
	10	2.49E-02	2.89E-03	2.77E-02
	20	9.94E-02	1.16E-02	1.11E-01
FG-O	2	1.01E-03	1.19E-04	1.13E-03
	5	6.29E-03	7.42E-04	7.03E-03
	10	2.51E-02	2.97E-03	2.81E-02
	20	1.01E-01	1.19E-02	1.12E-01
$v_{cnt}^* = 0.3, \zeta = 0.25, \xi = 0.4$				
UD	2	9.94E-04	1.16E-04	1.11E-03
	5	6.21E-03	7.22E-04	6.94E-03

	10	2.49E-02	2.89E-03	2.77E-02
	20	9.94E-02	1.16E-02	1.11E-01
FG-X	2	9.92E-04	1.15E-04	1.11E-03
	5	6.20E-03	7.19E-04	6.92E-03
	10	2.48E-02	2.88E-03	2.77E-02
	20	9.92E-02	1.15E-02	1.11E-01
		2	1.00E-03	1.17E-04
FG-O	5	6.25E-03	7.31E-04	6.98E-03
	10	2.50E-02	2.92E-03	2.79E-02
	20	9.99E-02	1.17E-02	1.12E-01
	$v_{cnt}^*=0.4, \zeta=0.25, \xi=0.4$			
UD	2	9.93E-04	1.15E-04	1.11E-03
	5	6.20E-03	7.20E-04	6.92E-03
	10	2.48E-02	2.88E-03	2.77E-02
	20	9.93E-02	1.15E-02	1.11E-01
FG-X	2	9.91E-04	1.15E-04	1.11E-03
	5	6.20E-03	7.17E-04	6.91E-03
	10	2.48E-02	2.87E-03	2.77E-02
	20	9.91E-02	1.15E-02	1.11E-01
FG-O	2	9.96E-04	1.16E-04	1.11E-03
	5	6.22E-03	7.25E-04	6.95E-03
	10	2.49E-02	2.90E-03	2.78E-02
	20	9.96E-02	1.16E-02	1.11E-01
$v_{cnt}^*=0.5, \zeta=0.25, \xi=0.4$				
UD	2	9.92E-04	1.15E-04	1.11E-03
	5	6.20E-03	7.19E-04	6.92E-03
	10	2.48E-02	2.87E-03	2.77E-02
	20	9.92E-02	1.15E-02	1.11E-01
FG-X	2	9.87E-04	1.14E-04	1.10E-03
	5	6.17E-03	7.14E-04	6.88E-03
	10	2.47E-02	2.86E-03	2.75E-02
	20	9.87E-02	1.14E-02	1.10E-01
FG-O	2	9.94E-04	1.16E-04	1.11E-03
	5	6.21E-03	7.22E-04	6.93E-03
	10	2.48E-02	2.89E-03	2.77E-02
	20	9.94E-02	1.15E-02	1.11E-01

Table 8. Comparison of the central deflection \bar{W} for the simply supported rectangular FG plates under three different combinations of hygrothermal loading with various aspect ratios along with varying CNT percentage (Partial Agglomeration Case-2):

CNT Pattern	b/h	SSSS		
		$\Delta T = 0, \Delta C = 10\%$	$\Delta T = 100, \Delta C = 0\%$	$\Delta T = 100, \Delta C = 10\%$
$v_{cnt}^*=0.05, \zeta=0.75, \xi=0.4$				
UD	2	1.02E-03	1.24E-04	1.15E-03
	5	6.40E-03	7.72E-04	7.18E-03
	10	2.56E-02	3.09E-03	2.87E-02
	20	1.02E-01	1.24E-02	1.15E-01
FG-X	2	1.01E-03	1.20E-04	1.13E-03
	5	6.33E-03	7.53E-04	7.08E-03
	10	2.53E-02	3.01E-03	2.83E-02
	20	1.01E-01	1.21E-02	1.13E-01
FG-O	2	1.08E-03	1.37E-04	1.22E-03
	5	6.73E-03	8.54E-04	7.58E-03
	10	2.69E-02	3.41E-03	3.03E-02
	20	1.08E-01	1.36E-02	1.21E-01
$v_{cnt}^*=0.075, \zeta=0.75, \xi=0.4$				
UD	2	1.01E-03	1.20E-04	1.13E-03
	5	6.33E-03	7.52E-04	7.08E-03
	10	2.53E-02	3.01E-03	2.83E-02
	20	1.01E-01	1.20E-02	1.13E-01
FG-X	2	1.00E-03	1.18E-04	1.12E-03
	5	6.28E-03	7.39E-04	7.02E-03
	10	2.51E-02	2.96E-03	2.81E-02
	20	1.00E-01	1.18E-02	1.12E-01

	2	1.05E-03	1.29E-04	1.17E-03
FG-O	5	6.53E-03	8.03E-04	7.33E-03
	10	2.61E-02	3.21E-03	2.93E-02
	20	1.04E-01	1.28E-02	1.17E-01
	$v_{cnt}^*=0.1, \zeta=0.75, \xi=0.4$			
UD	2	1.01E-03	1.19E-04	1.12E-03
	5	6.29E-03	7.42E-04	7.03E-03
	10	2.52E-02	2.97E-03	2.81E-02
	20	1.01E-01	1.19E-02	1.12E-01
FG-X	2	1.00E-03	1.17E-04	1.12E-03
	5	6.25E-03	7.33E-04	6.98E-03
	10	2.50E-02	2.93E-03	2.79E-02
	20	1.00E-01	1.17E-02	1.12E-01
FG-O	2	1.03E-03	1.25E-04	1.15E-03
	5	6.43E-03	7.78E-04	7.21E-03
	10	2.57E-02	3.11E-03	2.88E-02
	20	1.03E-01	1.24E-02	1.15E-01
$v_{cnt}^*=0.2, \zeta=0.75, \xi=0.4$				
UD	2	9.97E-04	1.16E-04	1.11E-03
	5	6.23E-03	7.27E-04	6.96E-03
	10	2.49E-02	2.91E-03	2.78E-02
	20	9.97E-02	1.16E-02	1.11E-01
FG-X	2	9.94E-04	1.15E-04	1.11E-03
	5	6.21E-03	7.22E-04	6.94E-03
	10	2.49E-02	2.89E-03	2.77E-02
	20	9.94E-02	1.16E-02	1.11E-01
FG-O	2	1.01E-03	1.19E-04	1.13E-03
	5	6.29E-03	7.43E-04	7.03E-03
	10	2.52E-02	2.97E-03	2.81E-02
	20	1.01E-01	1.19E-02	1.13E-01
$v_{cnt}^*=0.3, \zeta=0.75, \xi=0.4$				
UD	2	9.94E-04	1.16E-04	1.11E-03
	5	6.21E-03	7.22E-04	6.94E-03
	10	2.49E-02	2.89E-03	2.77E-02
	20	9.94E-02	1.16E-02	1.11E-01
FG-X	2	9.92E-04	1.15E-04	1.11E-03
	5	6.20E-03	7.19E-04	6.92E-03
	10	2.48E-02	2.88E-03	2.77E-02
	20	9.92E-02	1.15E-02	1.11E-01
FG-O	2	1.00E-03	1.17E-04	1.12E-03
	5	6.25E-03	7.32E-04	6.98E-03
	10	2.50E-02	2.93E-03	2.79E-02
	20	9.99E-02	1.17E-02	1.12E-01
$v_{cnt}^*=0.4, \zeta=0.75, \xi=0.4$				
UD	2	9.93E-04	1.15E-04	1.11E-03
	5	6.21E-03	7.20E-04	6.93E-03
	10	2.48E-02	2.88E-03	2.77E-02
	20	9.93E-02	1.15E-02	1.11E-01
FG-X	2	9.91E-04	1.15E-04	1.11E-03
	5	6.20E-03	7.17E-04	6.91E-03
	10	2.48E-02	2.87E-03	2.77E-02
	20	9.91E-02	1.15E-02	1.11E-01
FG-O	2	9.97E-04	1.16E-04	1.11E-03
	5	6.23E-03	7.26E-04	6.95E-03
	10	2.49E-02	2.90E-03	2.78E-02
	20	9.96E-02	1.16E-02	1.11E-01
$v_{cnt}^*=0.5, \zeta=0.75, \xi=0.4$				
UD	2	9.92E-04	1.15E-04	1.11E-03
	5	6.20E-03	7.19E-04	6.92E-03
	10	2.48E-02	2.87E-03	2.77E-02
	20	9.92E-02	1.15E-02	1.11E-01
FG-X	2	9.90E-04	1.15E-04	1.10E-03
	5	6.19E-03	7.16E-04	6.91E-03
	10	2.48E-02	2.86E-03	2.76E-02
	20	9.90E-02	1.15E-02	1.10E-01
FG-O	2	9.95E-04	1.16E-04	1.11E-03
	5	6.22E-03	7.23E-04	6.94E-03
	10	2.49E-02	2.89E-03	2.78E-02
	20	9.94E-02	1.16E-02	1.11E-01

Figure (10)-(15) is plotted to understand how CNT percentage affects the flexural response under a hygrothermal environment. Here as the CNT percentage increases the behavior is almost the same. The analysis results show that in all three combinations of hygrothermal loading the case where $\Delta T = 100$ and $\Delta C = 0\%$ shows the worst flexural response as deflection is higher compared to the other two cases as $\Delta T = 0$ and $\Delta C = 10\%$ & $\Delta T = 100$ and $\Delta C = 10\%$. The reference temperature and moisture coefficient are assumed to be zero in the analysis. The effect can be clearly understood from the stress diagram shown in Fig. (23)-(28), plotted against the thickness of the plate. The variation of in-plane normal and transverse stress shows that at the bottom there is no stress as compared to the top surface (as per Eq. 21 & 22).

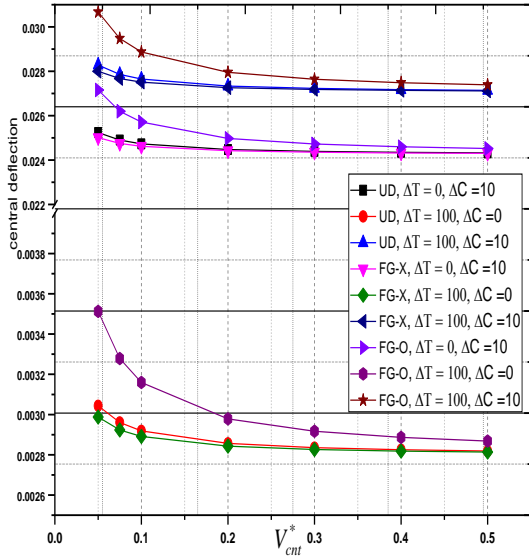


Fig. 10. Central deflection (\bar{w}) vs v_{cnt}^* under various combinations of Hygrothermal Effect ($b/h=10, \zeta=1, \xi=0.15$).

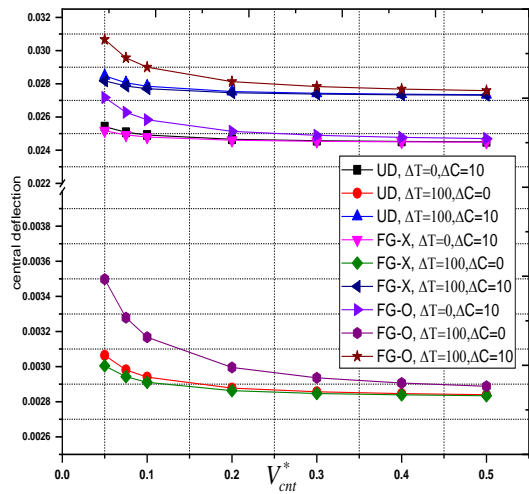


Fig. 11. Central deflection (\bar{w}) vs v_{cnt}^* under various combinations of Hygrothermal Effects ($b/h=10, \zeta=1, \xi=0.45$).

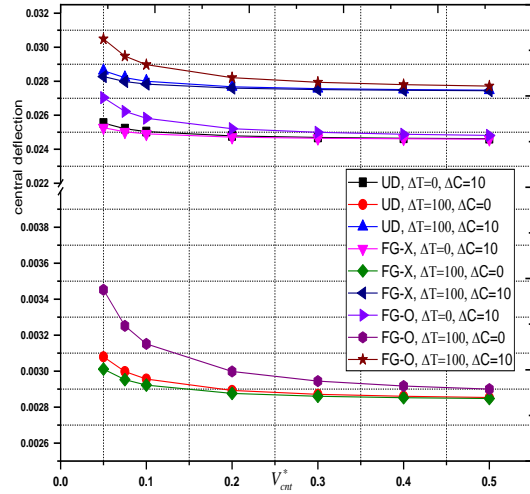


Fig. 12. Central deflection (\bar{w}) vs v_{cnt}^* under various combinations of Hygrothermal Effects ($b/h=10, \zeta=1, \xi=0.75$).

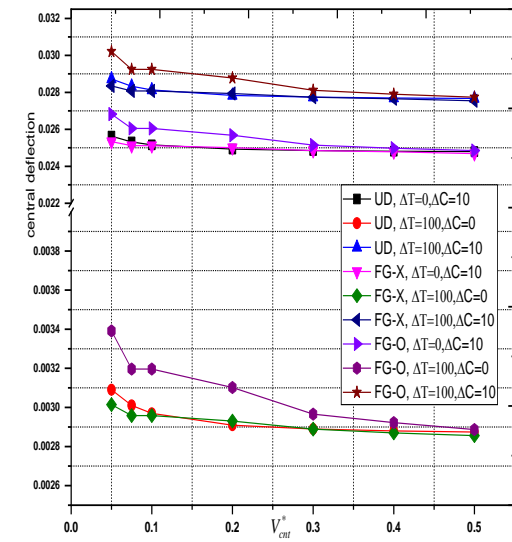


Fig. 13. Central deflection (\bar{w}) vs v_{cnt}^* under various combinations of Hygrothermal Effects ($b/h=10, \zeta=0.25, \xi=0.4$).

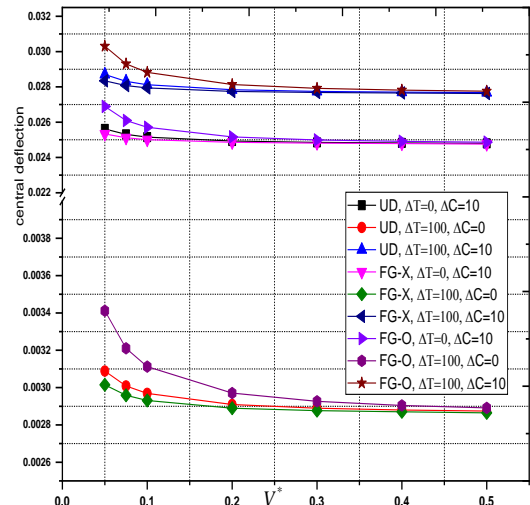


Fig. 14. Central deflection (\bar{w}) vs v_{cnt}^* under various combinations of Hygrothermal Effects ($b/h=10, \zeta=0.75, \xi=0.4$).

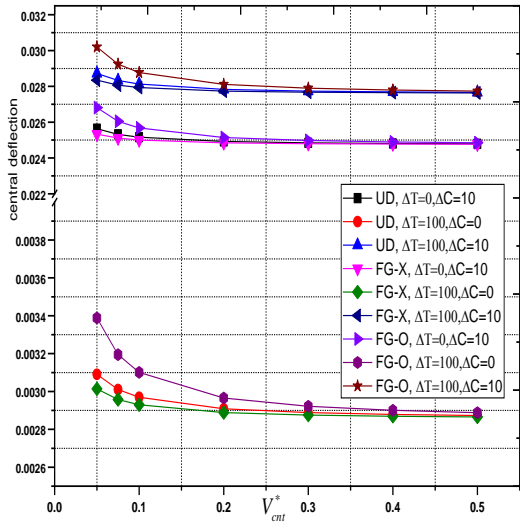


Fig. 15. Central deflection (\bar{w}) vs v_{cnt}^* under various combinations of Hygrothermal Effects ($b/h=10, \zeta=0.25, \xi=0.25$).

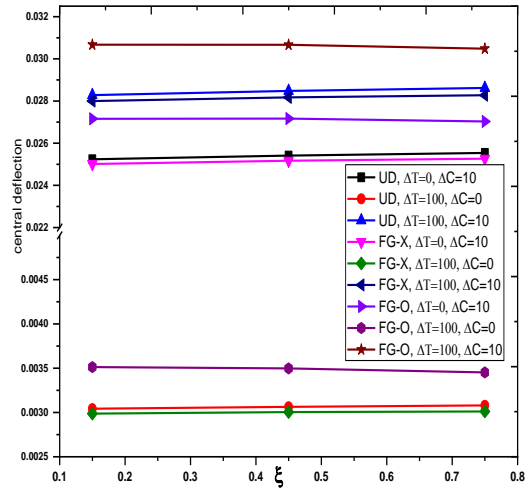


Fig. 16. Central deflection (\bar{w}) vs ξ under various combinations of Hygrothermal Effects for $v_{cnt}^*=0.05$ & $b/h = 10$.

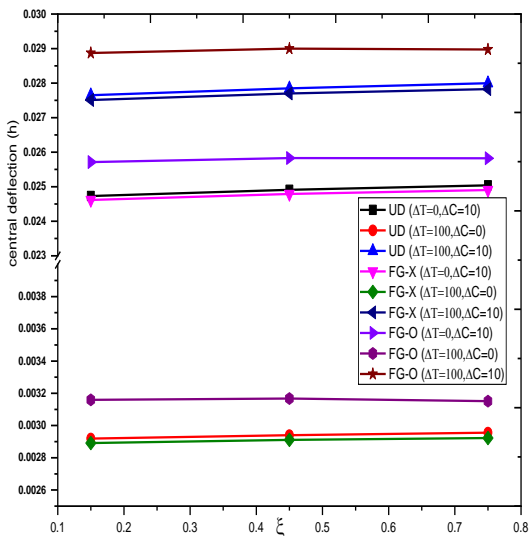


Fig. 17. Central deflection (\bar{w}) vs ξ under various combinations of Hygrothermal Effects for $v_{cnt}^*=0.1$ & $b/h = 10$.

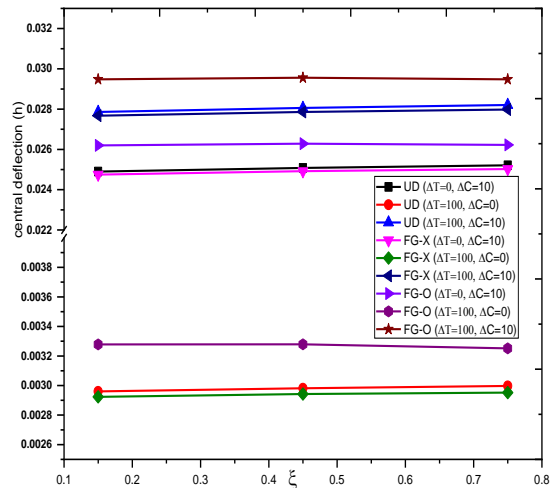


Fig. 18. Central deflection (\bar{w}) vs ξ under various combinations of Hygrothermal Effects for $v_{cnt}^*=0.075$ & $b/h = 10$.

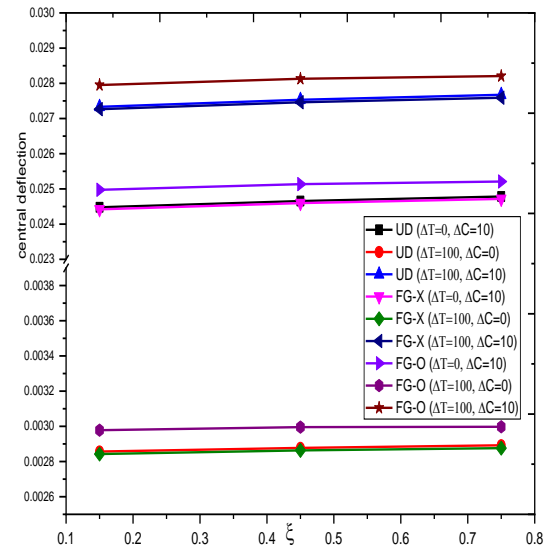


Fig. 19. Central deflection (\bar{w}) vs ξ under various combinations of Hygrothermal Effects for $v_{cnt}^*=0.2$ & $b/h = 10$.

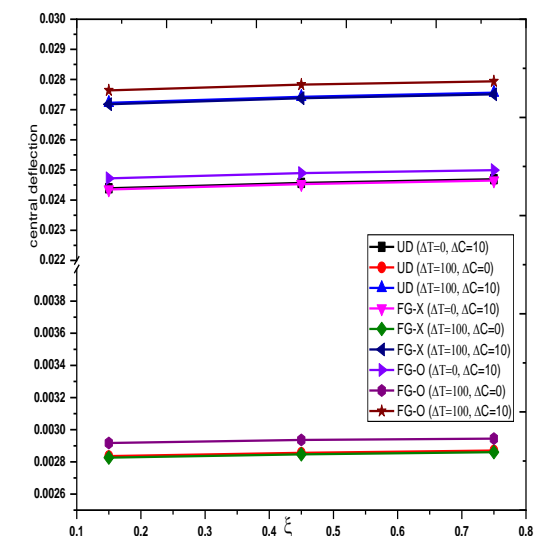


Fig. 20. Central deflection (\bar{w}) vs ξ under various combinations of Hygrothermal Effects for $v_{cnt}^*=0.3$ & $b/h = 10$.

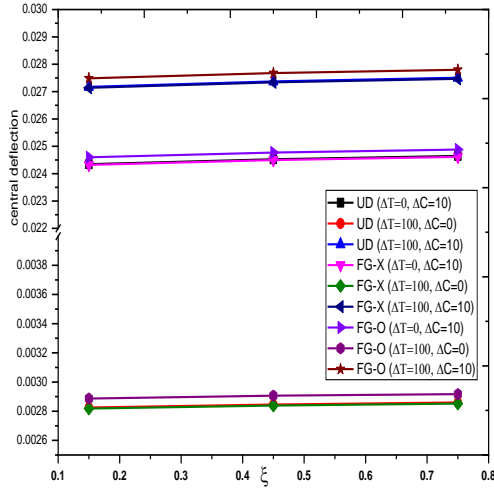


Fig. 21. Central deflection (\bar{w}) vs ξ under various combinations of Hygrothermal Effects for $v_{cnt}^* = 0.4$ & $b/h = 10$

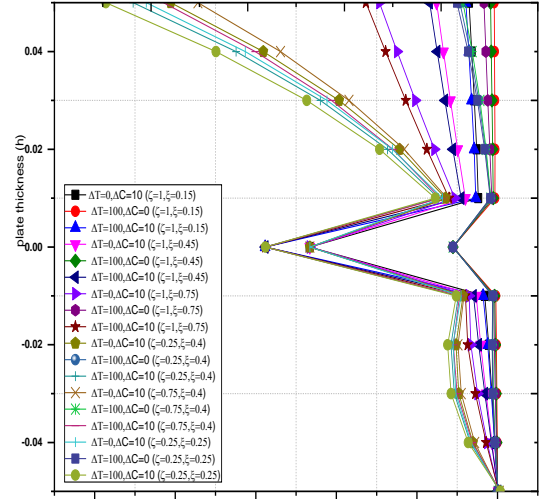


Fig. 24. In-plane normal stress (σ_{xx}) vs various combinations of Hygrothermal Effects for $b/h = 10$ & FG-X Type CNT pattern

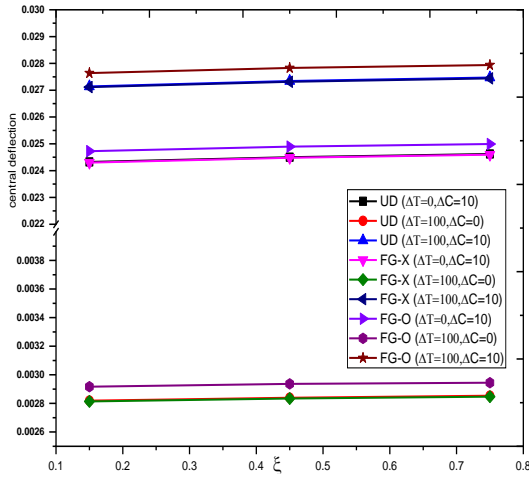


Fig. 22. Central deflection (\bar{w}) vs ξ under various combinations of Hygrothermal Effects for $v_{cnt}^* = 0.5$ & $b/h = 10$

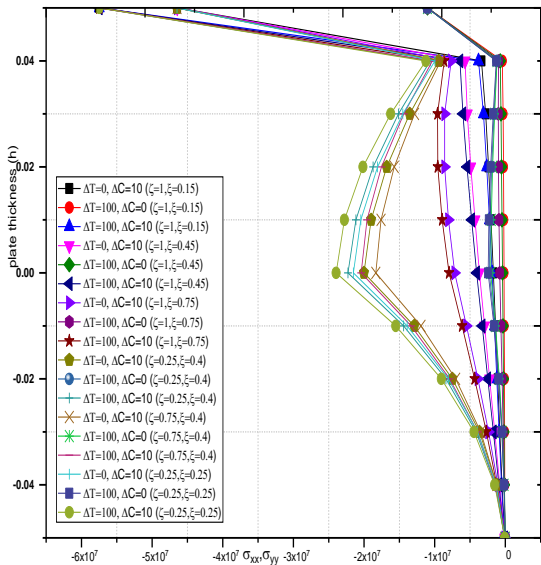


Fig. 25. In-plane normal stress (σ_{xx}) vs various combinations of Hygrothermal Effects for $b/h = 10$ & FG-O Type CNT pattern

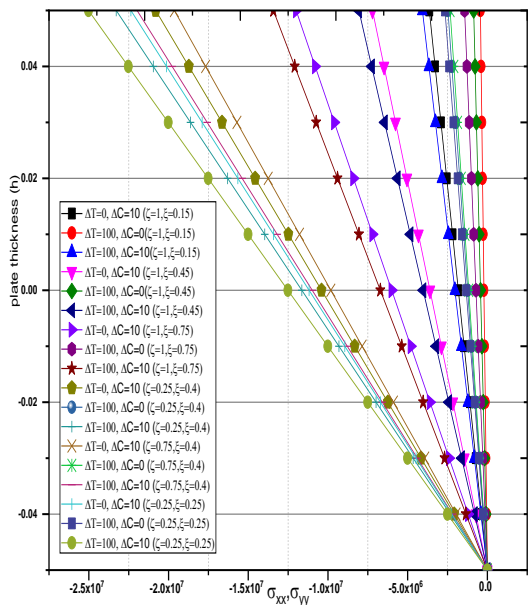


Fig. 23. In-plane normal stress (σ_{xx}) vs various combinations of Hygrothermal Effects for $b/h = 10$ & UD Type CNT pattern

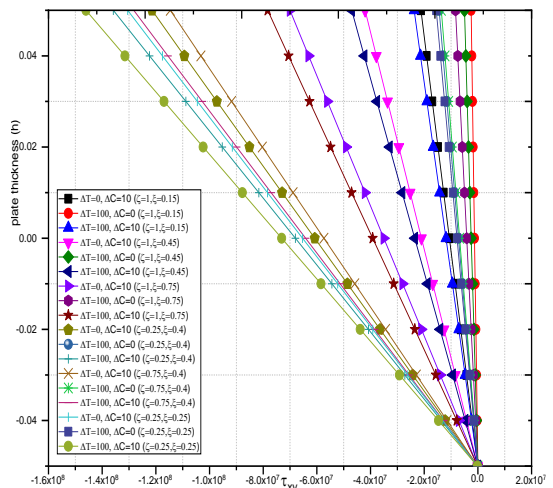


Fig. 26. Transverse shear stress (τ_{xy}) vs various combinations of Hygrothermal Effects for $b/h = 10$ & UD Type CNT pattern

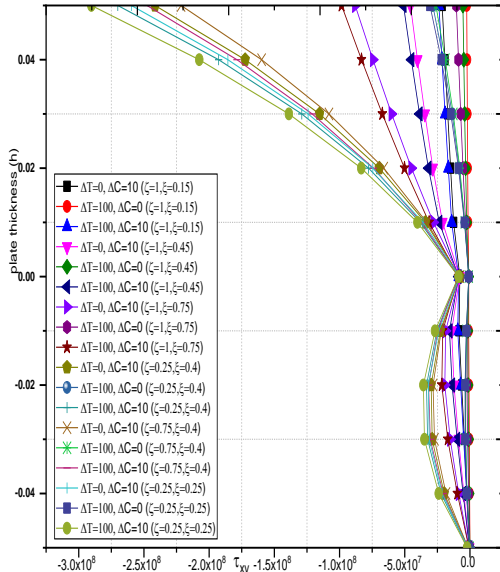


Fig. 27. Transverse shear stress (τ_{xy}) vs various combinations of Hygrothermal Effects for $b/h = 10$ & FG-X Type CNT pattern

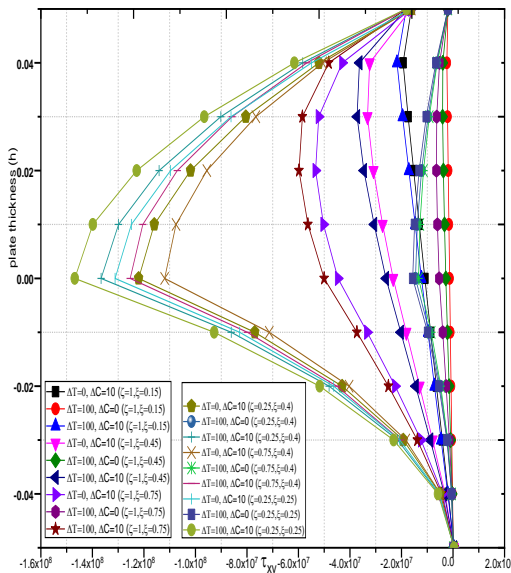


Fig. 28. Transverse shear stress (τ_{xy}) vs various combinations of Hygrothermal Effects for $b/h = 10$ & FG-O Type CNT pattern

6 Conclusions

In the current work, an investigation into the flexural behavior of nanocomposite plates under hygrothermal conditions, including the effect of agglomeration, was carried out using a C^0 FE model that was developed using Reddy's HSDT. It is presumed that the CNT distribution will be uniform or functionally graded. The Eshelby-Mori-Tanaka method is utilized in order to compute the properties of an agglomerated nanocomposite plate at any point. By adjusting these two parameters, it was possible to capture all three stages of the agglomeration effect. Several parametric studies were conducted to

determine the influence of reinforcing phase properties throughout the thickness, such as agglomeration and CNT distribution. These studies examine how these factors affect the flexural response of these structures.

The most important contribution of this work was the introduction of the carbon nanotube agglomeration model into the constitutive rules that define mechanical behavior. In addition, Reddy's well-known HSDT model is utilized in order to perform an analysis of the hygrothermal behavior of plates with varying parameters such as aspect ratio, CNT distribution across the thickness, and three distinct stages of agglomeration. Following is a summary of some important findings from a thorough examination of the hygrothermal flexural response and its sensitivity under various input parameters:

- When compared to the other two CNT distributions in the thickness direction that were considered for the same condition of aggregation, the FG-X type distribution of carbon nanotubes along the thickness direction gave a higher level of stiffness. This was the case irrespective of whether or not there was any agglomeration present, in any of the three separate instances of total agglomeration, or any of the two states of partial agglomeration. This is due to a larger concentration of carbon nanotubes in locations that experience significant levels of bending stress.
- According to the findings of the study, having a higher value for the parameter ξ causes the flexural behavior of these structures to worsen, which in turn results in higher flexural response for all other CNT distribution patterns.
- There is an increase in dimensionless central deflection with an increasing aspect ratio.
- The addition of clusters or regions of concentrated CNTs improves the flexural behavior of such models.
- The study shows that out of three hygrothermal loadings, the structure is more sensitive when only pure moisture conditions exist.
- The presence of a hygrothermal environment results in a decrease in the system's stiffness and flexural response, which is rational and consistent from a physical perspective.
- From the inplane stress diagram of three CNT variations (UD, FG-X & FG-O) across the thickness direction of the plate, one can easily understand that stress at the top is maximum while zero at the bottom

of the plate. The variation is as per Eq. 21 & 22 in which temperature and moisture at the bottom are assumed to be zero. Based on this three different combinations of hygrothermal loading are applied to investigate the static response of nanocomposite plate.

- Since the change in material properties across the thickness direction, there is a sudden jump in the stress diagram in FG-X and FG-O type CNT distribution pattern as compared to UD type CNT distribution.

Nomenclature

CNT	Carbon nanotube
FG	Functionally Graded Materials
h	Thickness
UD	Uniformly Distributed
V_{cnt}^*	Carbon nanotube volume fraction
SSSS	All four edges simply supported
FG-X	X-Type CNT distribution pattern along the thickness direction
FG-O	O-Type CNT distribution pattern along the thickness direction
ξ, ζ	Agglomeration parameter
N_i	Shape function
σ_{xx}, σ_{yy}	In-plane normal stress
τ_{xy}	Transverse shear stress

Acknowledgments

The funding for this work came from MMMUT, Gorakhpur U.P-273010 India, which the authors would like to thank.

Conflicts of Interest

The author declares that there are no conflict of interest regarding the publication of this manuscript.

References

[1] Iijima, S., 1991. Helical microtubules of graphitic carbon. *nature*, 354(6348), pp.56-58.

[2] Iijima, S. and Ichihashi, T., 1993. Single-shell carbon nanotubes of 1-nm diameter. *nature*, 363(6430), pp.603-605.

[3] Liew, K.M., Lei, Z.X. and Zhang, L.W., 2015. Mechanical analysis of functionally graded carbon nanotube reinforced composites: a review. *Composite Structures*, 120, pp.90-97.

[4] Aragh, B.S., Barati, A.N. and Hedayati, H., 2012. Eshelby–Mori–Tanaka approach for

vibrational behavior of continuously graded carbon nanotube-reinforced cylindrical panels. *Composites Part B: Engineering*, 43(4), pp.1943-1954.

- [5] Mareishi, S., Kalthori, H., Rafiee, M. and Hosseini, S.M., 2015. Nonlinear forced vibration response of smart two-phase nano-composite beams to external harmonic excitations. *Curved and Layered Structures*, 2(1).
- [6] Alibeigloo, A. and Liew, K.M., 2013. Thermoelastic analysis of functionally graded carbon nanotube-reinforced composite plate using theory of elasticity. *Composite Structures*, 106, pp.873-881.
- [7] Alibeigloo, A., 2014. Free vibration analysis of functionally graded carbon nanotube-reinforced composite cylindrical panel embedded in piezoelectric layers by using theory of elasticity. *European Journal of Mechanics-A/Solids*, 44, pp.104-115.
- [8] K.M. Liew, Z.Z. Pan, L.W. Zhang, The recent progress of functionally graded CNT reinforced composites and structures, *Science China Physics, Mechanics & Astronomy*, 63 (2020) 23460.
- [9] Liu, J., Cheng, Y., Xu, K., An, L., Su, Y., Li, X. and Zhang, Z., 2018. Effect of nano-silica filler on microstructure and mechanical properties of polydimethylsiloxane-based nanocomposites prepared by “inhibition-grafting” method. *Composites Science and Technology*, 167, pp.355-363.
- [10] Wang, M., Ma, L., Shi, L., Feng, P., Wang, X., Zhu, Y., Wu, G. and Song, G., 2019. Chemical grafting of nano-SiO₂ onto graphene oxide via thiol-ene click chemistry and its effect on the interfacial and mechanical properties of GO/epoxy composites. *Composites Science and Technology*, 182, p.107751.
- [11] Daghighi, V., Lacy Jr, T.E., Daghighi, H., Gu, G., Baghaei, K.T., Horstemeyer, M.F. and Pittman Jr, C.U., 2020. Heat deflection temperatures of bio-nanocomposites using experiments and machine learning predictions. *Materials Today Communications*, 22, p.100789.
- [12] Rafiee, R. and Shahzadi, R., 2018. Predicting mechanical properties of nanoclay/polymer composites using stochastic approach. *Composites Part B: Engineering*, 152, pp.31-42.
- [13] Irez, A.B., Bayraktar, E. and Miskioglu, I., 2018. Recycled and devulcanized rubber modified epoxy-based composites reinforced with nano-magnetic iron oxide, Fe₃O₄. *Composites Part B: Engineering*, 148, pp.1-13.
- [14] Meng, T., Yu, Y. and Wang, Z., 2017. Effect of nano-CaCO₃ slurry on the mechanical properties and micro-structure of concrete

- with and without fly ash. *Composites Part B: Engineering*, 117, pp.124-129.
- [15] Rathore, D.K., Prusty, R.K., Kumar, D.S. and Ray, B.C., 2016. Mechanical performance of CNT-filled glass fiber/epoxy composite in in-situ elevated temperature environments emphasizing the role of CNT content. *Composites Part A: Applied Science and Manufacturing*, 84, pp.364-376.
- [16] Bianco, A., Kostarelos, K. and Prato, M., 2005. Applications of carbon nanotubes in drug delivery. *Current opinion in chemical biology*, 9(6), pp.674-679.
- [17] Peer, D., Karp, J.M., Hong, S., Farokhzad, O.C., Margalit, R. and Langer, R., 2020. Nanocarriers as an emerging platform for cancer therapy. *Nano-Enabled Medical Applications*, pp.61-91.
- [18] Ghosh, S., Sood, A.K. and Kumar, N., 2003. Carbon nanotube flow sensors. *Science*, 299(5609), pp.1042-1044.
- [19] Snow, E.S., Perkins, F.K., Houser, E.J., Badescu, S.C. and Reinecke, T.L., 2005. Chemical detection with a single-walled carbon nanotube capacitor. *Science*, 307(5717), pp.1942-1945.
- [20] Tsukagoshi, K., Yoneya, N., Uryu, S., Aoyagi, Y., Kanda, A., Ootuka, Y. and Alphenaar, B.W., 2002. Carbon nanotube devices for nanoelectronics. *Physica B: Condensed Matter*, 323(1-4), pp.107-114.
- [21] Kempa, K., Rybczynski, J., Huang, Z., Gregorczyk, K., Vidan, A., Kimball, B., Carlson, J., Benham, G., Wang, Y., Herczynski, A. and Ren, Z.F., 2007. Carbon nanotubes as optical antennae. *Advanced Materials*, 19(3), pp.421-426.
- [22] Lau, K.T., Gu, C. and Hui, D., 2006. A critical review on nanotube and nanotube/nanoclay related polymer composite materials. *Composites Part B: Engineering*, 37(6), pp.425-436.
- [23] Fidelus, J.D., Wiesel, E., Gojny, F.H., Schulte, K. and Wagner, H.D., 2005. Thermo-mechanical properties of randomly oriented carbon/epoxy nanocomposites. *Composites Part A: Applied Science and Manufacturing*, 36(11), pp.1555-1561.
- [24] Han, Y. and Elliott, J., 2007. Molecular dynamics simulations of the elastic properties of polymer/carbon nanotube composites. *Computational Materials Science*, 39(2), pp.315-323.
- [25] Bonnet, P., Sireude, D., Garnier, B. and Chauvet, O., 2007. Thermal properties and percolation in carbon nanotube-polymer composites. *Applied Physics Letters*, 91(20), p.201910.
- [26] Coleman, J.N., Khan, U., Blau, W.J. and Gun'ko, Y.K., 2006. Small but strong: a review of the mechanical properties of carbon nanotube-polymer composites. *Carbon*, 44(9), pp.1624-1652.
- [27] Shi, D.L., Feng, X.Q., Huang, Y.Y., Hwang, K.C. and Gao, H., 2004. The effect of nanotube waviness and agglomeration on the elastic property of carbon nanotube-reinforced composites. *J. Eng. Mater. Technol.*, 126(3), pp.250-257.
- [28] Yu, J., Lacy Jr, T.E., Toghiani, H. and Pittman Jr, C.U., 2013. Effective property estimates for composites containing multiple nanoheterogeneities: Part II nanofibers and voids. *Journal of composite materials*, 47(10), pp.1273-1282.
- [29] Poursasghar, A., Yas, M.H. and Kamarian, S., 2013. Local aggregation effect of CNT on the vibrational behavior of four-parameter continuous grading nanotube-reinforced cylindrical panels. *Polymer Composites*, 34(5), pp.707-721.
- [30] Nejati, M., Asanjarani, A., Dimitri, R. and Tornabene, F., 2017. Static and free vibration analysis of functionally graded conical shells reinforced by carbon nanotubes. *International Journal of Mechanical Sciences*, 130, pp.383-398.
- [31] Kamarian, S., Salim, M., Dimitri, R. and Tornabene, F., 2016. Free vibration analysis of conical shells reinforced with agglomerated Carbon Nanotubes. *International Journal of Mechanical Sciences*, 108, pp.157-165.
- [32] Daghigh, H. and Daghigh, V., 2019. Free vibration of size and temperature-dependent carbon nanotube (CNT)-reinforced composite nanoplates with CNT agglomeration. *Polymer Composites*, 40(S2), pp.E1479-E1494.
- [33] Nasihatgozar, M., Daghigh, V., Eskandari, M., Nikbin, K. and Simoneau, A., 2016. Buckling analysis of piezoelectric cylindrical composite panels reinforced with carbon nanotubes. *International Journal of Mechanical Sciences*, 107, pp.69-79.
- [34] Moradi-Dastjerdi, R. and Malek-Mohammadi, H., 2017. Biaxial buckling analysis of functionally graded nanocomposite sandwich plates reinforced by aggregated carbon nanotube using improved high-order theory. *Journal of Sandwich Structures & Materials*, 19(6), pp.736-769.
- [35] Lei, Z.X., Liew, K.M. and Yu, J., 2013. Large deflection analysis of functionally graded carbon nanotube-reinforced composite plates by the element-free kp-Ritz method. *Computer Methods in Applied Mechanics and Engineering*, 256, pp.189-199.
- [36] Zhang, L.W. and Liew, K.M., 2015. Large

- deflection analysis of FG-CNT reinforced composite skew plates resting on Pasternak foundations using an element-free approach. *Composite Structures*, 132, pp.974-983.
- [37] Heydari, M.M., Hafizi Bidgoli, A., Golshani, H.R., Beygipoor, G. and Davoodi, A., 2015. Nonlinear bending analysis of functionally graded CNT-reinforced composite Mindlin polymeric temperature-dependent plate resting on orthotropic elastomeric medium using GDQM. *Nonlinear Dynamics*, 79(2), pp.1425-1441.
- [38] Mehar, K., Panda, S.K. and Patle, B.K., 2017. Thermoelastic vibration and flexural behavior of FG-CNT reinforced composite curved panel. *International Journal of Applied Mechanics*, 9(04), p.1750046.
- [39] Moghadam, H.Z., Faghidian, S.A. and Jamal-Omidi, M., 2018. Agglomeration effects of carbon nanotube on residual stresses in polymer nano composite using experimental and analytical method. *Materials Research Express*, 6(3), p.035009.
- [40] Ravari, M.K. and Zeighampour, H., 2015. Vibration analysis of functionally graded carbon nanotube-reinforced composite nanoplates using Mindlin's strain gradient theory. *Composite Structures*, 134, pp.1036-1043.
- [41] Phung-Van, P., Lieu, Q.X., Nguyen-Xuan, H. and Wahab, M.A., 2017. Size-dependent isogeometric analysis of functionally graded carbon nanotube-reinforced composite nanoplates. *Composite Structures*, 166, pp.120-135.
- [42] Thanh, C.L., Vu-Huu, T., Phung-Van, P., Nguyen-Xuan, H. and Abdel Wahab, M., 2018, August. Size-dependent analysis for FG-CNTRC nanoplates based on refined plate theory and modified couple stress. In *International Conference on Numerical Modeling in Engineering* (pp. 225-237). Springer, Singapore.
- [43] Rashidifar, M.A. and Ahmadi, D., 2015. Vibration analysis of randomly oriented carbon nanotube based on FGM beam using Timoshenko theory. *Advances in Mechanical Engineering*, 7(2), p.653950.
- [44] Mori, T. and Tanaka, K., 1973. Average stress in matrix and average elastic energy of materials with misfitting inclusions. *Acta metallurgica*, 21(5), pp.571-574.
- [45] Benveniste, Y., 1987. A new approach to the application of Mori-Tanaka's theory in composite materials. *Mechanics of materials*, 6(2), pp.147-157.
- [46] Shokrieh, M.M. and Rafiee, R., 2010. On the tensile behavior of an embedded carbon nanotube in polymer matrix with non-bonded interphase region. *Composite Structures*, 92(3), pp.647-652.
- [47] Yas, M.H. and Heshmati, M., 2012. Dynamic analysis of functionally graded nanocomposite beams reinforced by randomly oriented carbon nanotube under the action of moving load. *Applied Mathematical Modeling*, 36(4), pp.1371-1394.
- [48] Kamarian, S., Shakeri, M., Yas, M.H., Bodaghi, M. and Pourasghar, A., 2015. Free vibration analysis of functionally graded nanocomposite sandwich beams resting on Pasternak foundation by considering the agglomeration effect of CNTs. *Journal of Sandwich Structures & Materials*, 17(6), pp.632-665.
- [49] Khorasani, M., Lampani, L., Dimitri, R. and Tornabene, F., 2021. Thermomechanical Buckling Analysis of the E&P-FGM Beams Integrated by Nanocomposite Supports Immersed in a Hygrothermal Environment. *Molecules*, 26(21), p.6594.
- [50] Taj, M.G., Chakrabarti, A. and Sheikh, A.H., 2013. Analysis of functionally graded plates using higher order shear deformation theory. *Applied Mathematical Modeling*, 37(18-19), pp.8484-8494.
- [51] Moradi-Dastjerdi, R., Behdinan, K., Safaei, B. and Qin, Z., 2020. Buckling behavior of porous CNT-reinforced plates integrated between active piezoelectric layers. *Engineering Structures*, 222, p.111141.
- [52] Shinde, B.M., Sayyad, A.S. and Kawade, A.B., 2013. Thermal analysis of isotropic plates using hyperbolic shear deformation theory. *Applied and Computational Mechanics*, 7(2).
- [53] Reddy, J.N., 2003. *Mechanics of laminated composite plates and shells: theory and analysis*. CRC press.
- [54] Vinson, J.R., 2005. *Plate and panel structures of isotropic, composite and piezoelectric materials, including sandwich construction* (Vol. 120). Springer Science & Business Media.
- [55] Nasihatgozar, M., Daghigh, V., Lacy Jr, T.E., Daghigh, H., Nikbin, K. and Simoneau, A., 2016. Mechanical characterization of novel latania natural fiber reinforced PP/EPDM composites. *Polymer Testing*, 56, pp.321-328.
- [56] Daghigh, V., Lacy Jr, T.E., Pittman Jr, C.U. and Daghigh, H., 2018. Influence of maleated polypropylene coupling agent on mechanical and thermal behavior of latania fiber-reinforced PP/EPDM composites. *Polymer Composites*, 39(S3), pp.E1751-E1759.
- [57] Zhu, P., Lei, Z.X. and Liew, K.M., 2012. Static and free vibration analyses of carbon

- nanotube-reinforced composite plates using finite element method with first order shear deformation plate theory. *Composite Structures*, 94(4), pp.1450-1460.
- [58] Lei, Z.X., Liew, K.M. and Yu, J.L., 2013. Buckling analysis of functionally graded carbon nanotube-reinforced composite plates using the element-free kp-Ritz method. *Composite Structures*, 98, pp.160-168.
- [59] Mohammadimehr, M., Salemi, M. and Navi, B.R., 2016. Bending, buckling, and free vibration analysis of MSGT microcomposite Reddy plate reinforced by FG-SWCNTs with temperature-dependent material properties under hydro-thermo-mechanical loadings using DQM. *Composite Structures*, 138, pp.361-380.
- [60] Barai, P. and Weng, G.J., 2011. A theory of plasticity for carbon nanotube reinforced composites. *International Journal of Plasticity*, 27(4), pp.539-559.
- [61] Shen, L. and Li, J., 2004. Transversely isotropic elastic properties of single-walled carbon nanotubes. *Physical Review B*, 69(4), p.045414.
- [62] Odegard, G.M., Gates, T.S., Wise, K.E., Park, C. and Siochi, E.J., 2003. Constitutive modeling of nanotube-reinforced polymer composites. *Composites science and technology*, 63(11), pp.1671-1687.
- [63] Stephan, C., Nguyen, T.P., De La Chapelle, M. L., Lefrant, S., Journet, C. and Bernier, P., 2000. Characterization of single-walled carbon nanotubes-PMMA composites. *Synthetic Metals*, 108(2), pp.139-149.
- [64] Dai, T., Yang, Y., Dai, H.L., Tang, H. and Lin, Z.Y., 2019. Hygrothermal mechanical behaviors of a porous FG-CRC annular plate with variable thickness considering aggregation of CNTs. *Composite Structures*, 215, pp.198-213.
- [65] Brischetto, S., 2012. Hygrothermal loading effects in bending analysis of multilayered composite plates. *Computer Modeling in Engineering & Sciences(CMES)*, 88(5), pp.367-417.
- [66] Mahapatra, T.R. and Panda, S.K., 2016, February. Hygrothermal effects on the flexural strength of laminated composite cylindrical panels. In *IOP Conference Series: Materials Science and Engineering* (Vol. 115, No. 1, p. 012040). IOP Publishing.
- [67] Mahapatra, T.R., Panda, S.K. and Dash, S., 2016, September. Effect of hygrothermal environment on the nonlinear free vibration responses of laminated composite plates: A nonlinear Unite element micromechanical approach. In *IOP conference series: materials science and engineering* (Vol. 149, No. 1, p. 012151). IOP Publishing.
- [68] Daghighi, H., Daghighi, V., Milani, A., Tannant, D., Lacy Jr, T.E. and Reddy, J.N., 2020. Nonlocal bending and buckling of agglomerated CNT-reinforced composite nanoplates. *Composites Part B: Engineering*, 183, p.107716.
- [69] Dahiya, M. and Bansal, S.A., 2022. Graphene-reinforced nanocomposites: synthesis, micromechanics models, analysis and applications—a review. *Proceedings of the Institution of Mechanical Engineers, Part C: Journal of Mechanical Engineering Science*, 236(16), pp.9218-9240.
- [70] Shaikh, A.A., Pradhan, A.A., Kotasthane, A.M., Patil, S.S. and Karuppanan, S., 2022. Finite Element Analysis of Mechanical Properties of Basalt-Carbon Epoxy Hybrid Laminates. *Mechanics Of Advanced Composite Structures*, 9(2), pp.263-274.
- [71] Dwaikat, M.M.S., Spitas, C. and Spitas, V., 2012. Effect of the stochastic nature of the constituents parameters on the predictability of the elastic properties of fibrous nano-composites. *Composites science and technology*, 72(15), pp.1882-1891.
- [72] Georgantzinos, S.K., Antoniou, P.A. and Spitas, C., 2023. A multi-scale computational framework for the hygro-thermo-mechanical analysis of laminated composite structures with carbon nanotube inclusions. *Results in Engineering*, p.100904.
- [73] Chen, J., Khabaz, M.K., Ghasemian, M.M., Altalbawy, F.M., Jalil, A.T., Eftekhari, S.A., Hashemian, M., Toghraie, D. and Albahash, Z.F., 2023. Transverse vibration analysis of double-walled carbon nanotubes in an elastic medium under temperature gradients and electrical fields based on nonlocal Reddy beam theory. *Materials Science and Engineering: B*, 291, p.116220.
- [74] Alavi, S.M.R., Aghdam, M.M. and Eftekhari, A., 2006. Three-dimensional elasticity analysis of thick rectangular laminated composite plates using meshless local Petrov-Galerkin (MLPG) method. In *Applied Mechanics and Materials* (Vol. 5, pp. 331-338). Trans Tech Publications Ltd.
- [75] Maurya, M.C., Jawaid, S.M. and Chakrabarti, A., 2023. Free Vibration Response of Agglomerated Carbon Nanotube-Reinforced Nanocomposite Plates. *Mechanics Of Advanced Composite Structures*, 10(1), pp.167-194.